AFRL-RX-TY-TR-2013-0022

CHEMICAL AND BIOLOGICAL RESISTANT CLOTHING

Mickael Havel
Arkema, Inc
900 First Avenue
King of Prussia, PA 19406

Dale W. Schaefer and Naiping Hu
University of Cincinnati
University Hall, Suite 530
51 Goodman Drive, P.O. Box 21022
Cincinnati, OH 45221-0222

Tom Martin
Lion Apparel
7200 Poe Avenue, Suite 400
Dayton, OH 45414

Contract No. FA4819-11-C-0013

April 2013

AIR FORCE RESEARCH LABORATORY
MATERIALS AND MANUFACTURING DIRECTORATE

■ **Air Force Materiel Command** ■ **United States Air Force** ■ **Tyndall Air Force Base, FL 32403-5323**

DISCLAIMER

Reference herein to any specific commercial product, process, or service by trade name, trademark, manufacturer, or otherwise does not constitute or imply its endorsement, recommendation, or approval by the United States Air Force. The views and opinions of authors expressed herein do not necessarily state or reflect those of the United States Air Force.

This report was prepared as an account of work sponsored by the United States Air Force. Neither the United States Air Force, nor any of its employees, makes any warranty, expressed or implied, or assumes any legal liability or responsibility for the accuracy, completeness, or usefulness of any information, apparatus, product, or process disclosed, or represents that its use would not infringe privately owned rights.

NOTICE AND SIGNATURE PAGE

Using Government drawings, specifications, or other data included in this document for any purpose other than Government procurement does not in any way obligate the U.S. Government. The fact that the Government formulated or supplied the drawings, specifications, or other data does not license the holder or any other person or corporation; or convey any rights or permission to manufacture, use, or sell any patented invention that may relate to them.

This report was cleared for public release by the 88th Air Base Wing Public Affairs Office at Wright Patterson Air Force Base, Ohio available to the general public, including foreign nationals. Copies may be obtained from the Defense Technical Information Center (DTIC) (http://www.dtic.mil).

AFRL-RX-TY-TR-2013-0022 HAS BEEN REVIEWED AND IS APPROVED FOR PUBLICATION IN ACCORDANCE WITH ASSIGNED DISTRIBUTION STATEMENT.

///SIGNED///

KURT D. SILSBY, 1st Lt, USAF
Work Unit Manager

///SIGNED///

JOSEPH D. WANDER, PhD
Program Manager

///SIGNED///

DONNA L. PILSON, Lt Col, USAF
Deputy Chief, Airbase Technologies Division

This report is published in the interest of scientific and technical information exchange, and its publication does not constitute the Government's approval or disapproval of its ideas or findings.

REPORT DOCUMENTATION PAGE

Form Approved
OMB No. 0704-0188

PLEASE DO NOT RETURN YOUR FORM TO THE ABOVE ADDRESS.

1. REPORT DATE *(DD-MM-YYYY)*	2. REPORT TYPE	3. DATES COVERED *(From - To)*
09-APR-2013	Final Technical Report	28-SEP-2011 -- 28-FEB-2013

4. TITLE AND SUBTITLE

Chemical and Biological Resistant Clothing

5a. CONTRACT NUMBER

FA4819-11-C-0013

5b. GRANT NUMBER

5c. PROGRAM ELEMENT NUMBER

0909999F

6. AUTHOR(S)

*Havel, Mickael; **Schaefer, Dale W.; **Hu, Naiping; ***Martin, Tom

5d. PROJECT NUMBER

GOVT

5e. TASK NUMBER

L0

5f. WORK UNIT NUMBER

X0G2 (QL102028)

7. PERFORMING ORGANIZATION NAME(S) AND ADDRESS(ES)

*Arkema Inc, 900 First Avenue, King of Prussia, PA 19406
**University of Cincinnati, University Hall, Suite 530 51 Goodman Drive, P.O. Box 210222, Cincinnati, OH 45221-0222
***Lion Apparel, 7200 Poe Avenue, Suite 400, Dayton, OH 45414

8. PERFORMING ORGANIZATION REPORT NUMBER

9. SPONSORING/MONITORING AGENCY NAME(S) AND ADDRESS(ES)

Air Force Research Laboratory
Materials and Manufacturing Directorate
Airbase Technologies Division
139 Barnes Drive, Suite 2
Tyndall Air Force Base, FL 32403-5323

10. SPONSOR/MONITOR'S ACRONYM(S)

AFRL/RXQ

11. SPONSOR/MONITOR'S REPORT NUMBER(S)

AFRL-RX-TY-TR-2013-0022

12. DISTRIBUTION/AVAILABILITY STATEMENT

Distribution A: Approved for public release; distribution unlimited.

13. SUPPLEMENTARY NOTES

Ref Public Affairs Case # 88ABW-2013-3230; 15 July 2013. Document contains color images.

14. ABSTRACT

The research team composed of Arkema, Lion Apparel and University of Cincinnati (UC) successfully identified new barrier materials that exceed current technology for protective garments. These materials are novel semi-permeable membranes (SPMs) based on an amphiphilic block copolymers (BCPs) blended in a high-strength host polymer. This innovation was enabled by Arkema's Blocbuilder® controlled radical BCP polymerization technology, which generates tailored polymer architectures. The water transport properties and chemical warfare agent (CWA) rejection were measured at Arkema and UC. UC also developed characterization methods and computer simulation models to relate the permeation properties to the composition and nano scale morphology of the membranes.

15. SUBJECT TERMS

membrane, film, breathable, chemical resistance, biological resistance, selectivity

16. SECURITY CLASSIFICATION OF:			17. LIMITATION OF ABSTRACT	18. NUMBER OF PAGES	19a. NAME OF RESPONSIBLE PERSON
a. REPORT	b. ABSTRACT	c. THIS PAGE			Kurt Silsby
U	U	U	SAR	70	19b. TELEPHONE NUMBER *(Include area code)*

Reset

Standard Form 298 (Rev. 8/98)
Prescribed by ANSI Std. Z39.18

TABLE OF CONTENTS

LIST OF FIGURES

LIST OF TABLES

Page

ACKNOWLEDGEMENTS

Support for this project was provided by the DoD. The neutron reflectivity data were collected at Spallation Neutron Source (SNS) at Oak Ridge National Laboratory (ORNL). SANS data were collected using the General-Purpose Small-Angle Neutron Scattering Diffractometer at High Flux Isotope Reactor (HFIR) at Oak Ridge National Laboratory (ORNL). We thank Drs. James Browning and Ken Littrell for their support on data collection and analysis on the SANS and NR data. Research performed at SNS and HIFR at ORNL was sponsored by the Scientific User Facilities Division, Office of Basic Energy Sciences, U.S. Department of Energy.

1. SUMMARY

The research team composed of Arkema, Lion Apparel and University of Cincinnati (UC) successfully identified new barrier materials that exceed current technology for protective garments. These materials are novel semi-permeable membranes (SPMs) based on amphiphilic block copolymers (BCPs) blended in a high-strength host polymer. This innovation was enabled by Arkema's Blocbuilder® controlled radical BCP polymerization technology, which generates tailored polymer architectures. The water and chemical warfare agent (CWA) transport properties were measured at Arkema and UC. UC also developed characterization methods and computer simulation models to relate the permeation properties to the composition and nanoscale morphology of the membranes.

The new SPMs selectively transport moisture vapor (perspiration) while blocking ChemBio agents. In addition, the membranes maintain performance and mechanical integrity over a broad range of temperatures, resulting in a more protective and lighter weight garment than exists today. By comparison with the Military JSLIST combat garment, which implements the Saratoga carbon-absorption technology, the best performing candidates show a combination of high water vapor transmission rate (same level as JSLIST) and much higher water selectivity.

2. INTRODUCTION

Effective personal protection against exposure to toxic chemical agents in vapor form is critical in the military and in civilian defense due to threats of chemical-biological agents and industrial toxins.[1] Earlier technology was based on butyl rubber (i.e., linear poly(methylpropene-*co*-2-methyl-1,3-butadiene)), working on the principle of total blockage.[2] The lack of breathability of butyl rubber, however, results in fatigue and exhaustion due to heat stress and ineffective evaporative cooling.[1, 3]

To reduce the heat load, permeable clothing was developed implementing PBI Saratoga carbon pellet technology,[4,5] a carbonaceous-sorbent technology.[6] In this type of permeable clothing, a layer of finely distributed active carbon, either bound in polyurethane foam or as particles of carbon, is dispersed between two layers of textile. The highly porous, active-carbon layer permits water vapor released from the body to pass through, but adsorbs chemical warfare agents (CWAs) and thereby limits skin exposure.

The U. S. Department of Defense currently uses protective garments (Military JSLIST suit) made with three layers of open-cell polyurethane loaded with activated carbon.[1] These garments are bulky and heavy (PBI Saratoga weighs approximately 460 g/m^2).[5b] Therefore, lighter membranes are considered a high priority. In addition, protective garments based on activated carbon absorption are not effective against bio hazards or aerosols, are not suited for petroleum and oil environments, are not fire resistant, and have limited shelf and field service lifetimes.

Recent research in protective clothing seeks improved performance against the environment, thermo-physiological comfort, improved compatibility between and within different components in the clothing assembly, reduction in weight and bulk, ballistic protection, and reduction of life cycle costs.[7] High-performance nanofibers, highly functional and high-performance fabrics (including breathable fabrics by GORE-TEX® and laminated hydrophilic membranes) are emerging trends in protective clothing development.[7] Another promising area of development involves working enhanced SPMs using BCP blends in a host polymer. In this project we implemented the SPM strategy by synthesizing and identifying a group of copolymer blends to meet current JSLIST water permeation properties and display better CWA rejection.

3. METHODS AND PROCEDURES

3.1. BCP Synthesis

The technical approach utilized Arkema's proprietary BlocBuilder® MA controlled free-radical polymerization (CRP) to synthesize SPM BCPs that selectively transport moisture vapor (perspiration) while blocking ChemBio agents. BlocBuilder® MA technology has superior synthetic flexibility, providing greater capacity to tailor the composition of both the water-vapor-permeable (e.g., ionic or polar) and impermeable (i.e., structural and barrier) segments, enabling design and production of SPM materials with an improved balance of permeability and barrier properties. Based on reversible chain termination by a proprietary stable nitroxide radical called SG1 (Figure 1), this technology facilitates manufacture of controlled architecture polymers having precise molecular and chemical structures (e.g., controlled molecular weight, low polydispersity, controlled composition, and functional group placement) using standard industrial polymerization equipment.

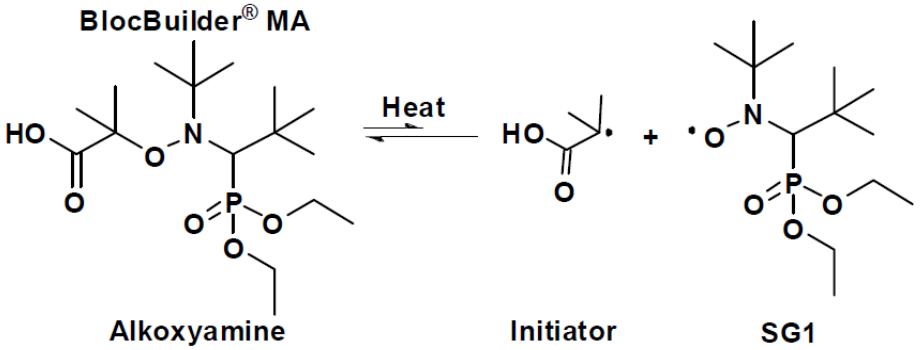

Figure 1. Chemical Structure of BlocBuilder®MA Alkoxyamine

BlocBuilder® MA controls free-radical polymerization of a broad selection of monomer types, including styrenic, acrylic, methacrylic, hydrophobic and low-surface-energy monomers; it is also highly tolerant of functional groups. This last feature is paramount for designing novel SPM BCPs as it not only allows for tailoring a given block's ionization level (e.g., sulfonation, phosphonation, etc.), but also the type and specific location—within the block segment—of the ionizable groups.

Access to such a vast array of functional monomers sets this technology apart from existing SPM BCPs, which are generally limited only to sulfonate groups, and thus provides access to novel SPM BCP structures with potentially improved properties. SPM BCP performance was improved by systematic investigation of judiciously selected parameters, such as chain architecture (e.g., AB diblock, ABA or BAB triblock), block composition, glass transition temperature, and molecular weight, type and location of ionic/hydrophilic and hydrophobic blocks, and block volume fractions.

Given the endless number of possible BCP architectures but limited amount of time, we focused our attention on enhancement of AB diblock architectures. Table 1 shows the functional monomers (coded) that we selected with their corresponding functions.

Table 1. Selected Monomers and Their Functions

Monomer	Nature	Function
A	Hydrophobic	Structural and thermal resistance, compatibility with host matrix
B	Hydrophobic	Structural and thermal resistance, processing aid
D	Hydrophobic	Structural and thermal resistance, processing aid
E	Hydrophobic	Flexibility
W1, W2	Hydrophilic	Water permeability

All synthetic experiments were conducted either in solvent or in bulk (i.e. the monomer is used as the solvent). The polymer length (molecular weight, M_n) was determined by adjusting the initiator concentration in the reaction media (equation (1)).

$$Mn(x) = Mn(\text{initiator}) + x * \frac{\left(\text{weight}_{\text{monomer(s)}}\right)_{t=o}}{\left(N_{\text{initiator}}\right)_{t=0}} \quad (1)$$

With
- x: conversion of monomer(s), dimensionless
- N: number of moles
- Mn: number average molecular weight, $g.mol^{-1}$

To obtain industrially viable BCPs, synthetic routes were adjusted to maximize yield. The overall yield is intimately related with the livingness (amount of polymer chains that can be further polymerized, i.e., that are terminated by an SG1 end group) of the first block. Throughout the report, special attention was dedicated to reaching the targeted polymer structure while maximizing yield (and thus livingness). Three routes were identified and investigated:

Route 1: Poly(A-co-B)–block–Poly(W1) , noted P(A-co-B)-b-P(W1)
Route 2: P(E-co-W1)–b-P(A) , in this route the hydrophilic block is synthesized first.
Route 3: P(E-co-W2)–b-P(A)

W1 is the hydrophilic monomer that was selected to make the second block. To improve yield and performance, W1 was polymerized both with and without additional co-monomers.

The first block, previously synthesized and consisting of a living P(A-co-B), is called the "macroinitiator" of the second block. Before proceeding to the polymerization of the second block, residual monomers were sometimes evaporated (trapped) from the macroinitiator solution. In all cases, a certain amount of residual monomer stayed in solution. Trapping involves stirring at high temperature and under vacuum, which can be detrimental to the polymer's livingness if run for a long time. The first block length was different in each polymer and variations in W1 concentration were evaluated.

All synthesis experiments were carried out using PARR pressure reactors equipped with a 1000-mL stainless steel vessel, regulated in temperature and pressure, operated under inert nitrogen atmosphere.

3.2. BCP Blend Membrane Preparation

3.2.1. Block Copolymer Blend Preparation at Arkema

3.2.1.1. Host Polymer Selection

Two families of polymer were chosen for making blends with the solution of diblock copolymer (coded):

- Hosts of type "N" were selected for their relatively high WVTR and compatibility with the newly synthesized BCPs. Three grades (same polymer with minor changes in comonomer ratio or molecular weight) of this host were tested, hereafter referred to as N1, N2, N3.
- Hosts of type "K" were selected for their extremely high chemical resistance and good compatibility with the newly synthesized BCP. Three grades of this host were tested, hereafter referred to as K1, K2, K3.

Advantages and disadvantages of these polymers are summarized in Table 2.

Table 2 Advantages and Disadvantages of Using N and K as Host Polymer

Polymer	Advantages	Disadvantages
N	Medium WVTR value (500–800 g/m^2.day at 37.8 °C); Good miscibility with P(A)	Low solubility in solvent/resins due to high viscosity
K	Excellent chemical resistance Good mechanical and thermal properties Excellent miscibility with P(A)	Very low WVTR (50 g/m^2.day at 37.8 °C) Low solubility in solvent (25% in NMP and only 8–10% in DMSO)

3.2.2. BCP Blend Membrane Preparation at UC

UC first established the blend membrane preparation procedure (see below). UC also investigated the effect of casting conditions on membrane properties, and concluded that the blade casting procedure generated more-uniform films than the free solvent casting method.

3.2.2.1. Solution Preparation

K1 solution was first prepared with 12 g of K1 powder in 100 mL of DMSO. After stirring for 24 h, the solution was degassed using evacuation for 1 h. Block copolymers were mixed with the K1 solution at a specific mixing ratio. The polymer blend was stirred for 45 min followed by degassing for 30 min. For more viscous block copolymers, the mixing and degassing times were increased to 1 h and 45 min, respectively.

3.2.2.2. Membrane Film Casting

K1–BCP blend films were cast by two methods. For the first method, dish casting (DC), a polymer blend was dropped into a flat-bottomed dish with an area of 58 cm^2. The dish was then cautiously moved to a level vacuum oven set at 90 °C. The oven was evacuated for 10 min after the dish was inserted into the oven. A cold trap was used to protect the pump during solvent evaporation. After casting for 40 min, the dish was retrieved. The hardened film was removed from the dish with a razor blade.

Most of the films in this study were cast using the blade casting (BC) method, in which a knife blade was used to spread the liquid over a flat glass plate. The area of the glass plate was

250 cm^2. The polymer blend had to be spread on the plate immediately before it was moved into the oven because a thickness gradient formed as soon as the solution was dispersed on the plate. For this method the casting time was extended to 50 min.

3.2.2.3. Annealing

UC investigated the effect of annealing temperature and type of substrate surface on film properties. Host polymers N2 and N3 were selected to carry out this study.

3.2.2.3.1. Annealing temperature

Two annealing temperatures were used (120 and 150 °C). At both temperatures, the films were placed in a vacuum oven overnight. A more uniform film resulted at 120 °C; treatment at 150 °C sometimes degraded portions of the films.

3.2.2.3.2. Substrate

Teflon and glass dishes were used as the substrate for annealing. Thin-film polymers annealed in Teflon dishes showed a patchy interface with some translucent regions. These translucent regions were not observed in unannealed films. Therefore we decided to cast all BCP blend films on glass plates.

3.3. Characterization

3.3.1. Permeation Tests

We measured single-gas permeability for water vapor and selected single gas molecules (e.g., H_2, N_2, O_2) through the films described above. The permeability (P_b) is the product of gas solubility (S) and diffusivity (D) in the polymer, i.e., $P_b = S \times D$. We conclude that for host polymer N2, the permeation mechanism is likely diffusion-limited for large molecules and sorption-limited for small molecules. The initial experimental data showed the N2 films to be highly selective toward water over the other single gases tested. The definition of flux (J_i, mol/m^2·s), permeance ($P_{m,i}$, mol/m^2·s·Pa) and permeability ($P_{b,i}$, mol m/m^2·s·Pa) are:

$$J_i = \frac{Q_i}{A_m t} \qquad (i = N_2, H_2O) \tag{2}$$

$$P_{m,i} = \frac{J_i}{\Delta P_i} \tag{3}$$

$$P_{b,i} = P_{m,i} \cdot \delta \tag{4}$$

where Q_i is the amount (mol) of gas permeating over a time period of t (s); A_m (m^2) is the active membrane area (2.54 cm^2 minus the area sealed by the O-ring seal); δ is the membrane thickness (m); and $\Delta P_i = (P_i)_f - (P_i)_p$, where $(P_i)_f$ and $(P_i)_p$ are the partial pressures (Pa) of the gas i upstream and downstream, respectively. The perm-selectivity (also called ideal selectivity) of water vapor over another gas ($\alpha^0_{H_2O/i}$) is defined as the ratio of pure gas permeances:

$$\alpha^0_{H2O/i} = \frac{P_{m,H_2O}}{P_{m,i}} \tag{5}$$

3.3.1.1. Humidity Chamber at Arkema

Small glass vials (~ 20 mL) were filled with deionized water (~ 17 g) to have a gap of 1.9 cm between the water surface and the film. Test cells were assembled by sandwiching polymer film between a glass vial and screw cap with a hole that allows most of the film area to be exposed to the water vapor. A gasket between the glass vial and the polymer film was also tested. All the glass vials were placed in a plastic box with desiccant solids (Drierite®) to control humidity in the box, Figure 2.

These experiments were carried out for a week to achieve an average of several measurements. Two membranes of each sample were analyzed simultaneously.

The humidity was regulated with a humidity controller. We tested a blank sample without a membrane to compare the results from different periods in the year (as relative humidity significantly varies in the lab environment throughout the year)

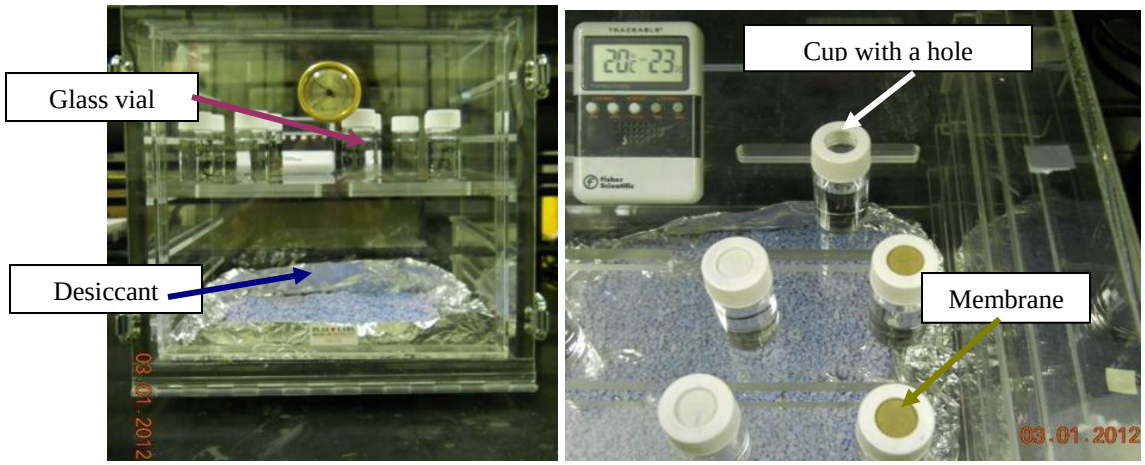

Figure 2. Pictures of the Plastic Box with Several Glass Vials Filled with Water

3.3.1.2. Mocon Permeatran 398

The Mocon Permeatran 398 was set up in a laboratory with humidity and temperature control. All samples (5 cm^2 area) were analyzed at different temperatures (usually 37.8 °C) . Each membrane was installed in the cell supported by an aluminum mask with one side at 100% relative humidity (RH, saturated sponge side), and the other side regulated at 10% RH (nitrogen purge flow side), Figure 3. Each cell was calibrated every week.

3.3.1.3. Acetone Permeation Test

An acetone permeation test was set up as a quick test to check the chemical resistance of the films. The permeation rate of acetone (1 wt %) through the membrane (diameter immersed = 4.10 cm) immersed in a solution of deionized water was tested, Figure 4. Evolution of the concentration of acetone penetrating was monitored versus time with a gas chromatography system and the permeation coefficient was calculated.

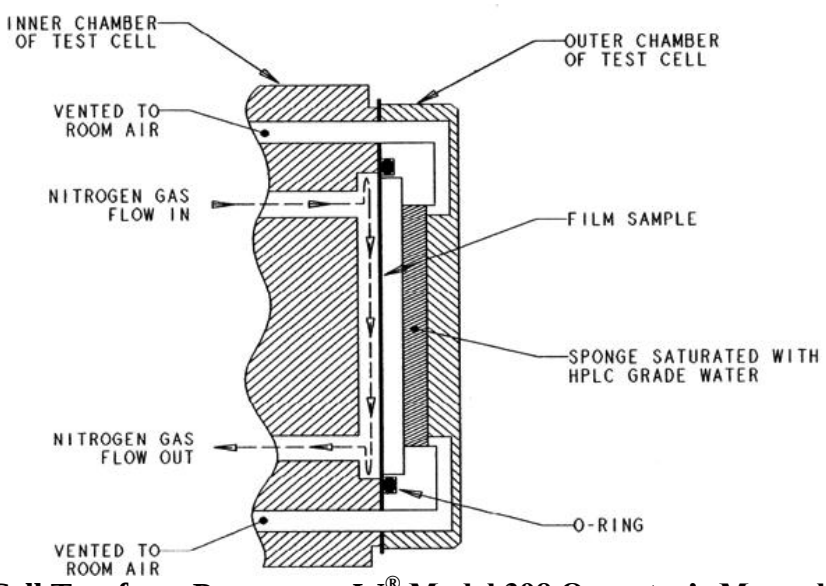

Figure 3. Cell Test from Permatran-W® Model 398 Operator's Manual, Sect. 1-5

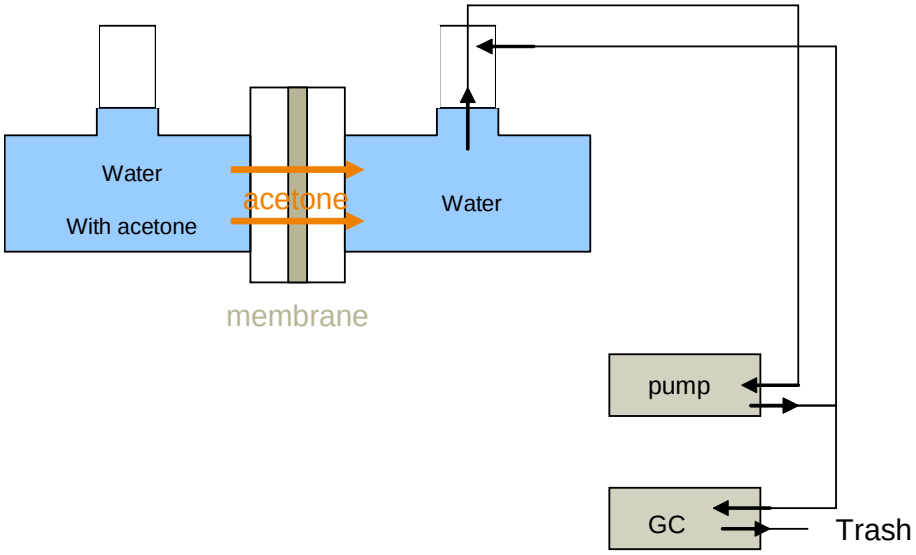

Figure 4. Acetone Permeation Test

3.3.1.4. Measurement of Room-temperature Permeability at UC

A cup method (Figure 5) was used to measure the water vapor permeance/permeability. This method adapts the ASTM E96 standard.[8] In particular, an air gap of 9–12 mm between the test liquid (water/chemical simulants) and the caps of the vials were maintained while loading all samples. A continuous airflow circulated through the humidity box after sweeping through two stages of drying by desiccants and molecular sieves, which allowed rapid lowering of RH in the box to 2~10 %, depending on the freshness of the desiccant.

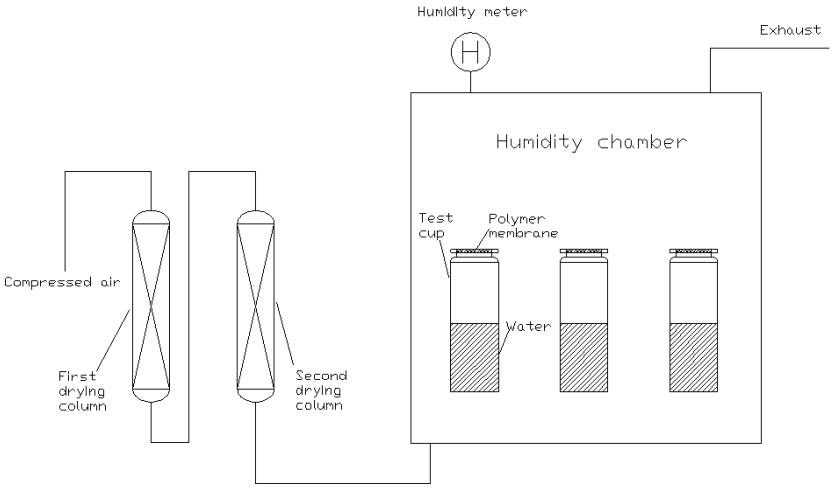

Figure 5. Measurement of Water/simulant Vapor Transport at Room Temperature

3.3.1.5. Single-gas Permeability

Single-gas permeance was measured for He, H_2, N_2, CH_4, *i*-C_4H_{10}, H_2O, and DMMP using the standard transient permeation method.[9] These gases/vapors were chosen to cover a range of molecular dynamic size, which is important for modeling considerations. The experimental apparatus for the transient gas permeation measurement is shown in Figure 6. The membrane was installed in a stainless steel cell and sealed by silicone *O*-rings. The upstream pressure was kept around 1~2 bar and the downstream side evacuated to less than 100 Pa before it was isolated for measurement of transient pressure increase in the gas tank. The permeance was calculated by the following equation:

$$P_{\mathrm{m}} = \frac{V_{\mathrm{c}}}{A_{\mathrm{m}} R T_0 \left(P' - P''\right)} \left(\frac{dP''}{dt} \right) \tag{6}$$

where V_c is the volume of the gas tank; A_m is the permeating area of the membrane, P' and P'' are pressures upstream and downstream of the membrane, respectively; T_0 is room (or tank) temperature, R is the gas constant and (dP''/dt) is the rate of pressure increase in the gas tank.

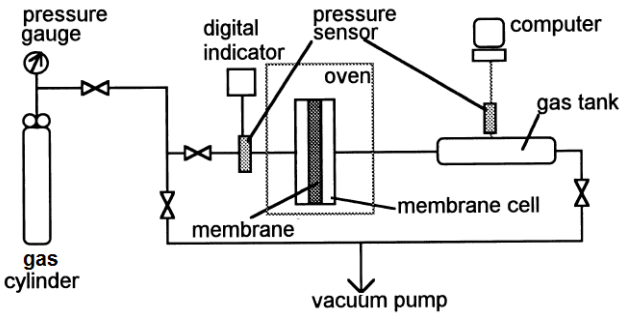

Figure 6. Schematic For Transient Single-Gas Permeation Measurements

3.3.1.6. High-temperature Water Permeability

The steady-state membrane permeation method was used to measure water vapor permeance through the polymer film (Figure 7). During the measurement, a helium gas flow bubbled

through a saturation column at room temperature and fed into one side of the membrane while the other side of the membrane was swept by a stream of pure helium. The sweep (permeate) stream exiting the membrane cell flowed through a sample collector immersed in liquid nitrogen to condense the water vapor completely. The amount of condensed water vapor was then weighed after a certain time of permeation. The water vapor permeance was determined based on the amount of the collected sample, the permeation time, and the difference in partial pressures of water between the feed and permeate sides.

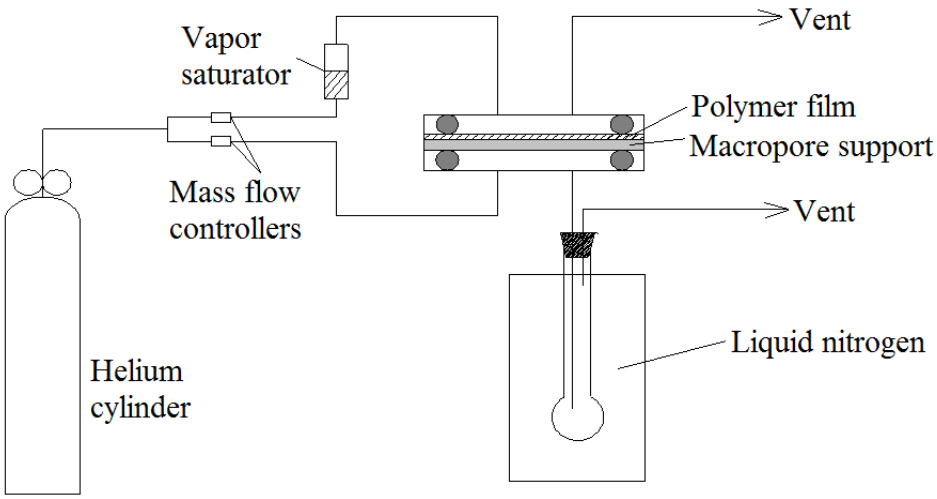

Figure 7. Schematic of Steady-State Water Permeation Test System

3.3.1.7. Water–DMMP Mixture Permeability

Permeation of water–DMMP vapor mixtures was studied using the steady-state vapor permeation system. Figure 8 shows a schematic of the experimental system. DMMP and water vapors saturated at room temperature were carried in helium flows (both flow rates were ~20 cm^3/min). The two gas flows were mixed and co-fed into the permeation cell (feed side) and the permeate side was swept by 40 cm^3/min of helium. The permeate gas stream passed through a liquid nitrogen cold trap to completely condense and collect the water and DMMP. The sample collected by the cold trap was weighed and then dissolved in isopropyl alcohol (IPA). An appropriate amount of dry zeolite-NaA particles (which is a nanoporous zeolite with composition of $[Na_{12}(H_2O)_{27}][Al_{12}Si_{12}O_{48}]$) as dehydrating agent was added to the solution to adsorb/remove water from the solution completely. The zeolite had a uniform pore diameter of ~0.41 nm, too small to accommodate DMMP molecules. Dehydration was confirmed by $CuSO_4$ (dry $CuSO_4$ turns light blue upon contacting water). The influence of DMMP adsorption on the zeolite external surface was confirmed to be negligible in calibration experiments. The zeolite-treated solution was then analyzed by gas chromatography (GC) to determine the amount of DMMP in the permeate mixture.

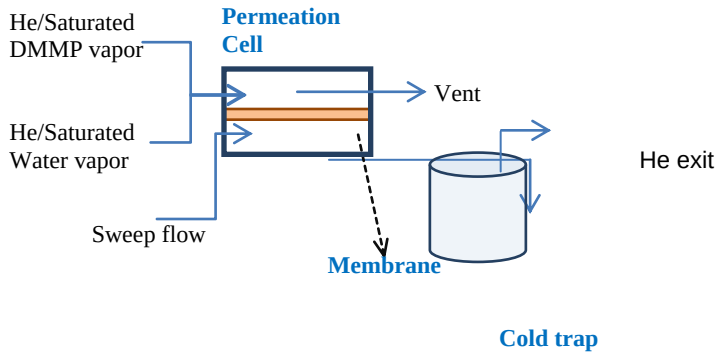

Figure 8. Water/DMMP Mixture Permeation System

3.3.1.8. Total Heat Loss (THL)

Moisture vapor transmission (MVTR) vs Total Heal Loss (THL): The MVTR test (MVTR) in accordance with ISO 15496 /15106-3 describes the water vapor permeability (WVP) of a fabric and therefore the rate of perspiration transport to the outside air. The measurements determined how many grams of moisture (water vapor) pass through a square meter of fabric in 24 h (the larger the value, the higher the breathability). For comparison purposes relating to comfort and chemical protection: the largest body of data that Lion has access to stems from our work with federal, state and local responders. These responders have established chemical protection requirements that include consideration of the physiological effects on the responders from long-duration events. The consensus performance requirements mentioned below utilize a blend of dry and wet comfort factors to deliver a "Total Heat Loss" number. THL measurements per ASTM F1868, Part C are required by the following:

- National Fire Protection Association (NFPA) standards:
  - NFPA 1971: Standard on Protective Ensembles for Structural Fire Fighting and Proximity Fire Fighting (2007)
  - NFPA 1951: Standard on Protective Ensembles for Technical Rescue Incidents (2007)
  - NFPA 1977: Standards on Protective Clothing and Equipment for Wildland Fire Fighting (2011)
  - NFPA 1994: Standard on Protective Ensembles for First Responders to CBRN Terrorism Incidents (2007)
  - NFPA 1999: Standards on Protective Clothing for Emergency Medical Operations (2008)

Comfort—Total Heat Loss: A primary function of clothing is comfort. Clothing comfort is often defined as the absence of discomfort, and perceptions of discomfort are sensed when clothing materials impede the flow of heat and moisture from the body.

Measurement of a material's ability to transfer both body heat and moisture into a designated environmental condition is done using sweating skin instrumentation. The guarded sweating hot plate measures heat flow from the calibrated test plate (heated to a skin surface temperature of 35 °C) through the material into the test environment (25 °C, 65% RH), and is determined for both simulated dry and wet skin conditions.

The sweating skin instrumentation, when used in a dry state, measures dry heat transfer with outputs used to calculate thermal resistance/insulation values. Following the dry test, the instrument is fed water and made to "sweat." The instrument, when used in a sweating state, uses the heat transfer results to calculate evaporative resistance. These measurements also provide a picture of the permeability, breathability, and heat loss from sweat evaporation.

Measurements obtained from both the dry and wet test plates were combined to calculate total heat loss (RHL) in W/m². THL is the heat transferred through the test material from a fully sweating test plate surface into the test environment. THL, measured at a 100% wet skin condition, indicates the highest predicted metabolic activity level that a wearer may sustain and still maintain body thermal comfort while in a highly stressed state in the test environment. Because, the sweating hot plate does not consider effects such as insulating air layers, garment design or fit, the THL value represents the highest theoretically possible amount of heat that can be transferred through a material system for a given set of environmental conditions without active cooling or ventilation.

All heat and moisture transfer properties were calculated from measurements of thermal transport made with the large skin model hot plate instrumentation. These measurements were made in accordance with the requirements of ASTM F1868 and/or ISO 11092.

3.3.2. Polymer Characterization

For polymer characterization (polymer composition, chemical structure), several techniques were used.

3.3.2.1. Calculation of Global Monomer Conversion

The monomer(s) conversion was calculated with the following equation (7):

$$x = \frac{[M]_0 - [M]_t}{[M]_t} = 1 - \frac{[M]_t}{[M]_0} \tag{7}$$

With | $[M]_0$ initial monomer conversion
$[M]_t$ monomer conversion at time t

The extend of conversion of each monomer in the copolymerization mixture was obtained by GC (monomer soluble in THF) or by HPLC (monomer soluble in DMSO, W1 conversion).

In all cases, the initial sample (media with monomers and solvent) was analyzed. For calculating each individual conversion, the disappearance of each monomer in the media was monitored. For a certain time, the individual conversion was calculated with this equation:

$$X_A = 1 - \frac{(I_A)_t}{(I_A)_0} \tag{8}$$

With | X_A individual conversion of monomer A
$(I_A)_0$ amount of monomer A detected by HPLC or GC at initial time
$(I_A)_t$ amount of monomer A detected by HPLC or GC at time t

So, the global weight conversion, x_w can be calculated with (9), where m_A and m_B are the initial weights introduced in the monomers mixture,

$$x_w = X_A \times w_{A,0} + X_B \times w_{B,0} \text{ with } w_{A,0} = \frac{m_A}{m_A + m_B} \text{ and } w_{B,0} = \frac{m_B}{m_A + m_B} \quad (9)$$

The global molar conversion, x_n, is calculated with (10), where n_x is the initial moles of monomers introduced in the mixture:

$$x_n = X_A \times f_{A,0} + X_B \times f_{B,0} \text{ with } f_{A,0} = \frac{n_A}{n_A + n_B} \text{ and } f_{B,0} = \frac{n_B}{n_A + n_B} \quad (10)$$

3.3.2.2. Gas Chromatography (GC)

GC analyses were performed with an Agilent 6850 series GC system in THF under hydrogen flow and the flame ionization detector (FID) was calibrated with a standard solution. All polymers were analyzed at a concentration of 10 mg/mL with a butyl acetate internal standard (elution time at 3.85 min) at the same concentration after filtration through a 0.45-μm polytetrafloroethylene (PTFE) membrane filter.

The GC tracked the conversion of each monomer (soluble in THF) during the synthesis by monitoring its concentration at different times during polymerization.

3.3.2.3. High-performance Liquid Chromatography (HPLC)

The samples were analyzed with an Agilent Model 1100 liquid chromatography system equipped with a UV detector at room temperature. The system was equipped with an Agilent Poroshell 120 EC-C_{18}, 50 mm × 3.0 mm × 2.6 μm column. The flow rate was 0.8 mL/min and the injection volume was 1.0 μL. A calibration was done before each run. All polymers were analyzed at a concentration of 3–6 mg/mL in DMSO solution after filtration through a 0.45-μm PTFE membrane. The mobile phase for sample elution consisted of solvent A (0.1% H_3PO_4 in water) and solvent B (0.1% H_3PO_4 in methanol) for at least 1 h. After each run, the column was washed with a 50/50 solution of IPA and water at a rate of 0.2 mL/min.

3.3.2.4. Size Exclusion Chromatography (SEC)

SEC analyses were performed with a Waters Alliance™ chromatographic system at 50 °C in DMSO containing 0.1 mol % $NaNO_3$ at a flow rate of 1 mL. All polymers were analyzed at a concentration of 5–10 mg/mL after filtration through a 0.45-μm PTFE membrane. The separation was carried out on two PFG linear XL columns with a particle size of 7 μm (Polymer Standards Service). The setup was equipped with a refractive index (RI) detector (model 2414, sensitivity = 64). The average molar masses (number-average, M_n, and weight-average, Mw) and the polydispersity index (PDI = M_w/M_n) were derived from the RI signal by a calibration curve based on polyW1 (PW1) standards. The software used for data collection and calculation was Empower Pro version 5.0 from Waters.

3.3.2.5. ^{31}P Nuclear Magnetic Resonance (NMR)

d_6-DMSO was added to all samples to provide a lock signal. All spectra were collected at 25 °C. ^{31}P NMR spectra were collected on a Bruker AV400 spectrometer equipped with a 10-mm Broad Band Observe (BBO) probe.

Phosphorus NMR is an analytical technique for tracking the livingness of these copolymers. To synthesize a multiblock copolymer, we need to attach the SG1 function at the end of each chain. This moiety contains a ^{31}P nucleus, which can be detected by ^{31}P NMR. Homolytic separation of SG1 initiates polymerization of the second block. The ^{31}P NMR measurement identifies the amount of material available for the second block polymerization.

3.3.2.6. ^{13}C NMR

The ^{13}C NMR measures the chemical composition of the diblock copolymers. d_6-DMSO was added to samples as a lock signal. All spectra were collected at 25 °C. Spectra were collected on the Bruker AV400 using a 10-mm BBO probe..

3.3.2.7. Glass Transition Temperature (T_g) measurement

We measured the T_gs for BCP samples N2 and N3 host polymers using differential scanning calorimetry (DSC). The thermal stability of these polymers at high temperature (annealing temperature) was also tested by thermo gravimetric analysis (TGA).

3.3.2.8. Small-angle Neutron Scattering

Small-angle neutron scattering (SANS) measures the nanoscale phase separation that is responsible for the unique properties of these block copolymers. The nature of this phase separation is determined by the block ratios and compositions as well as by the film deposition conditions. Both the size scale and the morphology (sheets, rods, spheres) of the domains impact transport and needed be taken into account in modeling transport phenomena.

SANS is very sensitive to the presence of deuterium, so by exposing the films to heavy water vapor (D_2O) we were able to track the ingress of water into the film and determine the evolution of the domain morphology as a function of BCP composition and blending ratio.

SANS was performed at the CG-2 beamline at the High Flux Isotope Reactor (HIFR) at Oak Ridge National Laboratory (ORNL; Oak Ridge, TN, USA). Scattering data were collected as the scattered intensity versus the modulus of the momentum transfer wave vector, q. Specifically we measured the differential scattering cross section per unit volume on an absolute scale, which is referred to as the intensity, $I(q)$. The data were subject to Unified-fit using the Argonne National Laboratory routines in Irena macros package.[10]

3.3.2.9. Neutron Reflectivity (NR)

Neutron reflectivity (NR) was used to elucidate the interfacial structure of cast BCP films. NR is used to probe the density and chemical composition change at interfaces and reveals how BCP phase separation is affected by casting. Upon exposure to D_2O, NR revealed the location of the hydrophilic phase relative to the interface position.
In the NR experiments, each sample was irradiated by the incident neutron beam at a very small incident angle, θ. The ratio of the fluxes of the reflected beam to the incident beam was measured as a function of scattering vector, q. The relationship between θ and q is

$$q = \frac{4\pi \sin\theta}{\lambda} \tag{11}$$

where λ is the wavelength of the incident beam. For NR, θ is fixed and a broad spectrum of wavelengths impinges on the sample (1.5 Å $<\lambda<$ 16 Å), to obtain a range of q values. The actual λ of any particular detected neutron is calculated by time of flight.

The normalized reflected intensity (R) is plotted against q. The Rq curve results from the superposition of waves scattered by the interface. The amplitude and attenuation of each wave are determined by the thickness, roughness and scattering length density (SLD) of each layer. Thickness and roughness represent structural information while the SLD reveals the chemical composition:

$$\text{SLD} = \rho \frac{N_A}{M} \sum\nolimits_{\text{molecule}} b_i \tag{12}$$

where ρ is the mass density, N_A is Avogadro's number, M is the molecular weight, b_i is the atomic scattering length of atom i, and $\rho \frac{N_A}{M}$ is molecular number density. $\sum_{\text{molecule}} b_i$ is the sum over scattering lengths of all atoms present in one molecule.

The R–q data were analyzed using Irena macros 2.35 for Igor Pro 6.20 to extract the SLD profile (SLD as function of perpendicular distance from substrate). Neutron reflectivity was performed using the Liquids Reflectometer (LR), Spallation Neutron Source (SNS) at ORNL.

3.3.2.10. Small-Angle X-ray Scattering (SAXS)

Samples were analyzed by SAXS to better understand their morphology as a function of temperature (24 °C, 38 °C) and RH (40%, 90%). SAXS measurements were conducted on the x-ray scattering instrument at the Laboratory for Research on the Structure of Matter (LRSM) facility at the University of Pennsylvania using the environmental chamber.

Radiation Cu K_α, 40 kV, 85 mA. Distance from the chamber to the detector = 150 cm.

Exposure time = 600–900 s. Bruker–Nonius FR-591 rotating anode (0.2- × 0.2-mm² filament, ~0.3 mm² on sample). Pinhole collimation slits (3) with confocal Max-Flux optics. Bruker AXS Hi-Star multiwire area detector.

Data manipulation was done using the datasqueeze software v2.1.9. Scattering data were obtained by averaging integrated intensities with the following *q (scattering vector)* and χ (rotation angle around the x-ray beam axis) ranges:

$$Q = [7\times10^{-3}; 0.14] \text{ with } 5\times10^{-4} \text{ steps. } \chi = [-120°; +220°]$$

3.3.3. Modeling of Structure–property Relationship

3.3.3.1. Hansen Solubility Parameter Calculation

The permeation mechanism of water vapor and chemical simulants was first investigated by comparison of water/DMMP permeability to those of single-gas molecules. The single-gas

permeability was obtained using the apparatus described in Figure 6. The sorption component (S) in permeability ($P = D \times S$, where D is the diffusion coefficient) is associated to the Hansen solubility parameter.[11]

A group-contribution-based sorption model was developed that calculates the Hansen solubility parameter (HSP) from the chemical composition of the BCPs. Empirical parameters from a literature database[11] were used in this model. Parameters from experiments and molecular simulation were calculated to set up a database valid for PMMA-based BCPs.

$$\delta_t^2 = \frac{E_{coh}}{V_m} = \frac{\Delta H_{vap} - RT}{V_m} \tag{13}$$

$$\delta_t^2 = \delta_d^2 + \delta_p^2 + \delta_h^2 \tag{14}$$

$$\Delta\delta_{BCP,Water} = \sqrt{4\left(\delta_d^{BCP} - \delta_d^{Water}\right) + 4\left(\delta_p^{BCP} - \delta_p^{Water}\right) + 4\left(\delta_h^{BCP} - \delta_h^{Water}\right)} \tag{15}$$

$$\Delta\delta_{BCP,DMMP} = \sqrt{4\left(\delta_d^{BCP} - \delta_d^{DMMP}\right) + 4\left(\delta_p^{BCP} - \delta_p^{DMMP}\right) + 4\left(\delta_h^{BCP} - \delta_h^{DMMP}\right)} \tag{16}$$

where E_{coh} is the cohesive energy density of the BCP, ΔH_{vap} is the heat of evaporation of the BCP, V_m is the molecular volume of the BCP chain, δ_t is the total HSP, and δ_t, δ_p, and δ_h are the dispersion, polar, and hydrogen bonding components of the total HSP, respectively. Solubility of water and DMMP can be predicted by Eq. (15) and Eq. (16), respectively. The higher the values from Eqs (15) and (16), the higher the solubility of water or DMMP is in this BCP. Selectivity of water/DMMP is the ratio of Eqs (15) and (16).

3.3.3.2. Molecular Dynamic Simulation

Molecular dynamics and grand canonical Monte Carlo (GCMC) simulation were used to predict solubility based on sorption isotherms for single-gas molecules. The solubility, therefore, was used to validate the model and establish the database. The COMPASS force field (Condensed-phase Optimized Molecular Potentials for Atomistic Simulation Studies) [12] was used for all simulations. The simulation results were used to understand the water and DMMP permeation mechanism and to calculate energy parameters for the database to use in HSP calculations (for specific groups for which energies terms were unavailable in literature).

First, chains of BCPs with 200 repeat units were prepared using an initial *cis–trans* conformation. The COMPASS force field and the charge group method for electrostatic interactions were used. The polymer chain was minimized for 1000 steps and used to construct a periodic amorphous cell using the explicit image convention. Based on a conventional rotational isomeric state (RIS) model, a stepwise chain construction scheme using the torsion potential obtained from COMPASS generated the initial structure. A 100-step minimization process was used to refine the resulting cells and eliminate any bad contacts (overlapping or close contacts of atoms). This process was followed by an annealing procedure during which the periodic cell was heated from 300 to 600 K at intervals of 50 K and then cooled back to 298 K. At each step of the cycle, the cells were subjected to 50 ps (ps = picoseconds) of NPT (fixed values of number of atoms, pressure and temperature) dynamics. Next, a 50-ps interval of dynamics at fixed values of

number of atoms, volume and temperature was used to further relax the polymer structure with the cell density fixed at the average value obtained from the 50-ps NPT dynamics calculation. This sequence was followed by an additional 150 ps of NPT dynamics. The first 50 ps of dynamics were discarded and the remaining 100 ps were saved as a history file. The polymer cell was used for GCMC simulation of solubility at 298 K. Single-gas (He, N_2, CH_4, CO_2, and *i*-C_4H_{10}, H_2O and DMMP vapor) concentrations were determined at pressure increments of 1 kPa over a range from 0 to 12 kPa. A total of 200,000 steps were used for each gas sorption measurement.

3.3.3.3. Diffusion Correction Based on Domain Size

The domain size affects the diffusivity coefficients of both water and chemical simulants, and therefore the permeability and selectivity. In BCP–K1 blend systems, the difference between hydrophilic and hydrophobic domain sizes determined the diffusion components of the selectivity parameter. In general, the effect of domain size on diffusivity is determined by

$$\frac{D_{\mathrm{m}}}{D_0} = \left(1 - \frac{R_{\mathrm{s}}}{R_{\mathrm{p}}}\right)^n \tag{17}$$

where D_{m} and D_0 are the diffusivity before and after correction by porous size, R_{s} is the diameter of permeate, and R_{p} is the diameter of domain size, n is an empirical parameter that is often given the value 4.0.

4. BENCHMARK CURRENT TECHNOLOGIES AND EXISTING MATERIALS

4.1. Current Technologies

Current technologies for biochemical-resistant clothing include PBI Saratoga carbon pellet technology and semi-permeable membranes. Permeability and selectivity have been investigated for representative samples using both technologies (JSLIST military garment as PBI Saratoga and GoreTex/ChemPak as semi-permeable membranes). Room temperature MVTR and selectivity (water/DMMP) of JSLIST, ChemPak XRT, and ChemPak Ultra Barrier are presented in Figure 9.

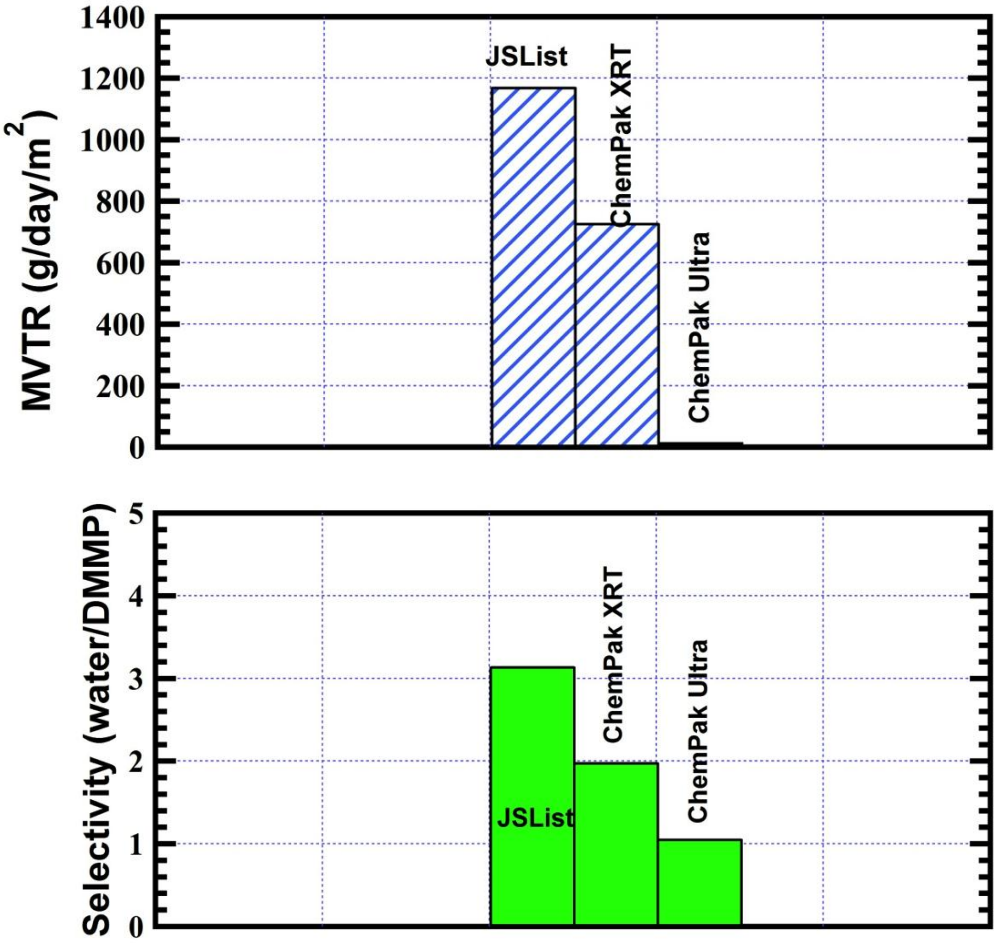

Figure 9. MVTR (top) and Selectivity (Water/DMMP) (bottom) of JSLIST, ChemPak XRT and ChemPak Ultra Barrier

4.1.1. Existing Commercial Arkema BCPs (P1, P2, L1, L2, and N2, N3)

Water and DMMP transport rates and selectivity of several Arkema commercial brands were evaluated. Their performances are summarized and compared to JSLIST in Figure 10.

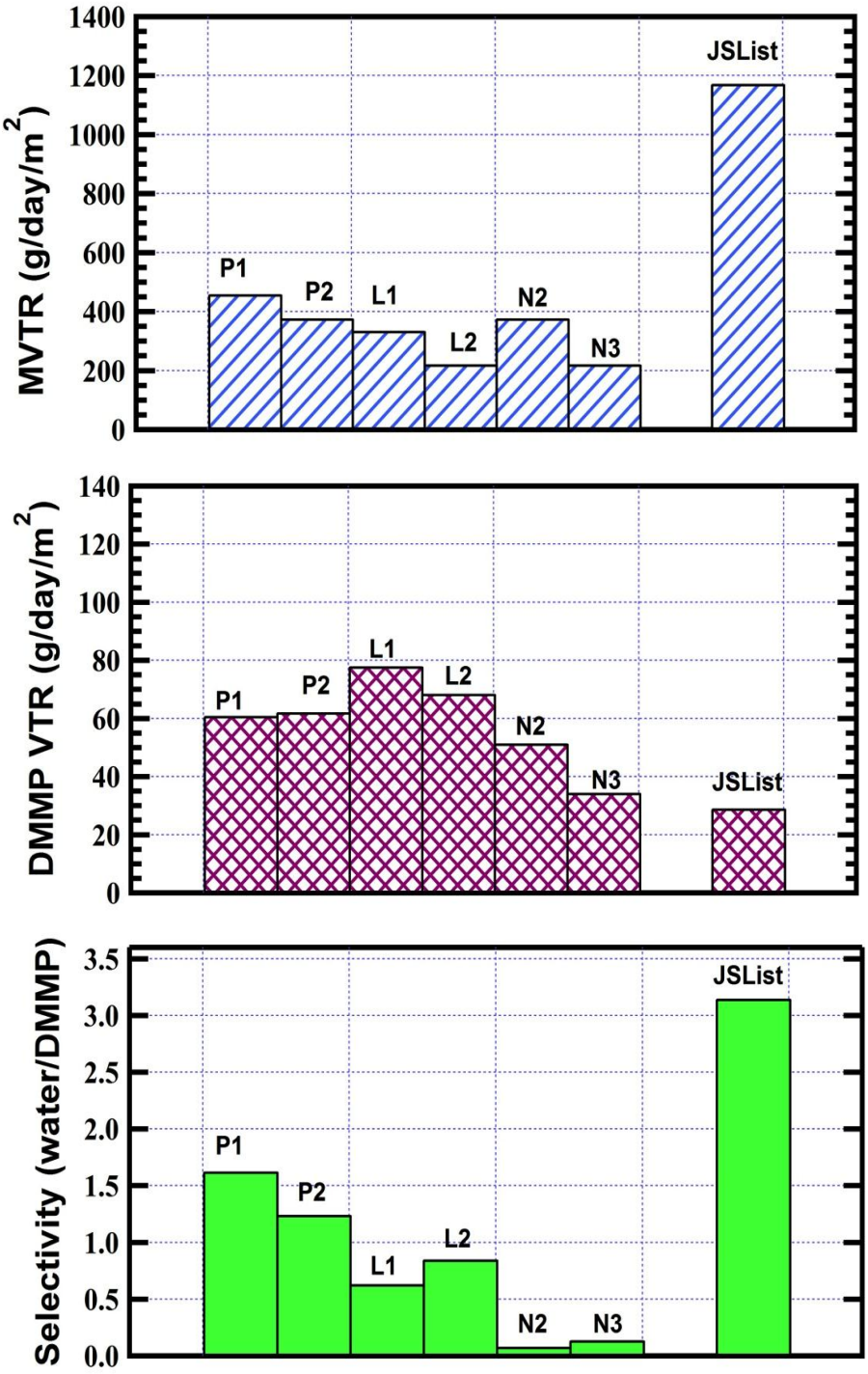

Figure 10. MVTR and Selectivity (Water/DMMP) of Arkema Commercial Brands Compared with JSLIST

5. BLOCK COPOLYMER SYNTHESIS AND CHARACTERIZATION

5.1. Block Copolymer Synthesis

5.1.1. Route 1: P(A-co-monomer)-b-P(W1)

For this route, the first block was a P(A-co-B)-based copolymer in which A and B were randomly copolymerized. It is important to note that a high level of livingness of the first block was desired to permit restarting the polymerization to obtain the second block. This concept was a strong driver for all improvements to polymerization conditions thereafter.

5.1.1.1. First Block: P(A-co-B)

Co-monomer B was necessary to maintain good control over the polymerization of A. However, B was detrimental to the BCP's compatibility with the potential host matrices. Therefore, the concentration of B was adjusted in the media (with the same initiator amount) to identify the minimal amount of B necessary. The livingness percentage and conversion rate were used to monitor the reaction (Table 3). Percentage of livingness was tracked by adding an inert compound, triphenyl phosphite (TPPO), as an internal standard in the mixture. Comparing the intensity of its signal to that of TPPO permitted is to use NMR to follow the disappearance of SG1 bonded to polymer chains.

Table 3. Route 1—First block: P(A-co-B); Effect of B concentration

Expt.	$[A]_0$ mol/L	$[B]_0$ mol/L	$W_{B,0}$	Livingness %	Conversion[a] %
BCP 48	3.7	4.3	0.5	-	68
BCP 24	3.9	2.45	0.35	55	55
BCP 12	3.9	1.5	0.25	34	51

[a] weight global conversion calculated obtained by GC and HPLC.

5.1.1.2. Diblock: P(A-co-B)-b-P(W1-co-monomer)

W1 was the hydrophilic monomer selected for the second block. To improve yield and performance W1 was polymerized both with and without additional co-monomer. The first block, previously synthesized, and consisting of a living P(A-co-B) was called a "macroinitiator" of the second block. Before proceeding to the polymerization of the second block, residual monomers were sometimes evaporated (trapped) from the macroinitiator solution. In all cases, a certain amount of residual monomers remained in solution. Note that trapping involves stirring at high temperature and under vacuum, which can be detrimental to the polymer's livingness if run for a long time. The first block length was different in each polymer and variations in W1 concentration were evaluated.

5.1.1.2.1 P(A-co-B)-b-PW1 with partial trap of residual monomers, $M_n^{\text{First block}}$= 1 AU (Arbitrary Unit)

W1 polymerizations were run in DMSO at 100–120 °C with a varying macroinitiator concentrations -P(A-co-B)-SG1- in a 2-L reactor. The different polymerizations of W1 were initiated by a macroinitiator solution, P(A-co-B)-SG1, which contained 50 wt% B and had M_w = 1 AU, Table 7.

Table 4. Route 1 to Diblock: P(A-co-B)-b-PW1; M_n First block = 1 AU

Expt.	First block	[First block]$_0$ mol/L	[W1]$_0$ mol/L	M_n diblock (AU)	Conversion[a)] %
BCP 84	BCP 82	3.7×10^{-3}	0.55	2.5	90
BCP 88	BCP 82	5.1×10^{-3}	0.78	2.2	97
BCP 109	BCP 104	6.3×10^{-3}	0.35	2.5	99
BCP 115	BCP 104	3.9×10^{-3}	0.41	3.5	97

[a)] Weight global conversion calculated obtained by GC and HPLC.

The W1 concentration in the reaction did not impact the global weight conversion or number-average molar mass evolution (Figure 11 (a) and (b)). The PDI stayed below 1.5. These experiments allowed us to synthesize four BCPs with same first block length but with different amounts of W1.

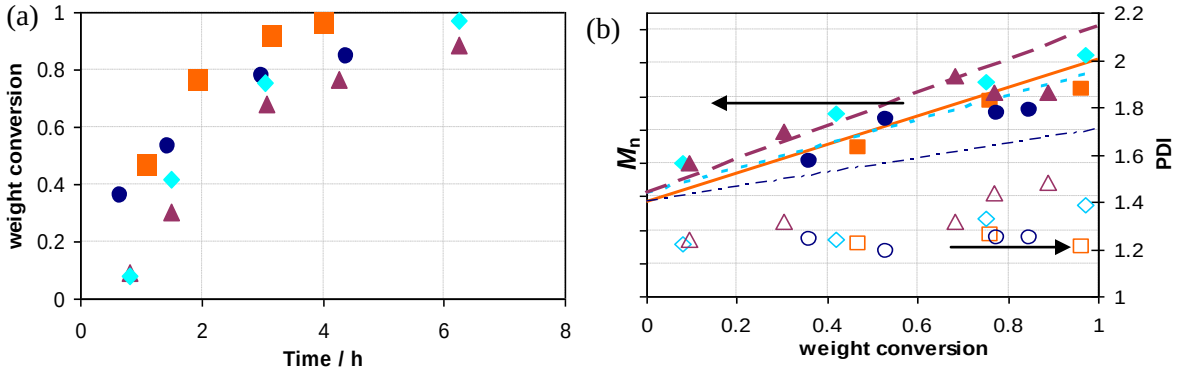

Figure 11. Polymerization of (W1)

▲(BCP 84, BCP 82 initiator), ◊ (BCP 88, BCP 82 initiator), ● (BCP 109, BCP 104 initiator), ■ (BCP 115, BCP 104 initiator), (a) Overall weight conversion obtained by GC and HPLC vs time and (b) M_n (full symbols) and PDI = Mw/ M_w/M_n (corresponding empty symbols) with a solid and dashed lines for M_n^{theo} values.

5.1.2. Route 2: P(E-co-W1)-b-P(A)

With this route, the hydrophilic block P(W1) or its copolymers were synthesized first. The use of E as a co-monomer assures high livingness with high conversion rates at the end of the polymerization. With this new route, a final conversion of 70~80% was obtained.

W1 polymerizations were done in either water or DMSO. Several copolymerizations of P(W1-co-E) were also conducted in DMSO. In a second step, these different first block solutions (still containing small amounts of residual monomer), were used as macroinitiators to polymerize the second block P(A).

5.1.2.1. First Block: P(W1)

W1 homopolymerizations were conducted in water or in DMSO. The living characters of these syntheses were tracked by ^{31}P NMR.

W1 was polymerized in DMSO at 95–100 /°C, initiated by BlocBuilder® MA. This process was easier than the surfactant-free emulsion process because both blocks of the diblock copolymer were soluble in DMSO, Table 5.

Table 5. Route 2 to First block: P(W1) in DMSO

Expt.	$[W1]_0$ Mol/L	Conversion[a)] %
BCP 38	1.3	17
BCP 39	1.3	17
BCP 51	1.3	97

[a)] weight global conversion calculated from GC and HPLC data.

The global conversion evolutions were slow for two polymerizations, Figure 12 (a).

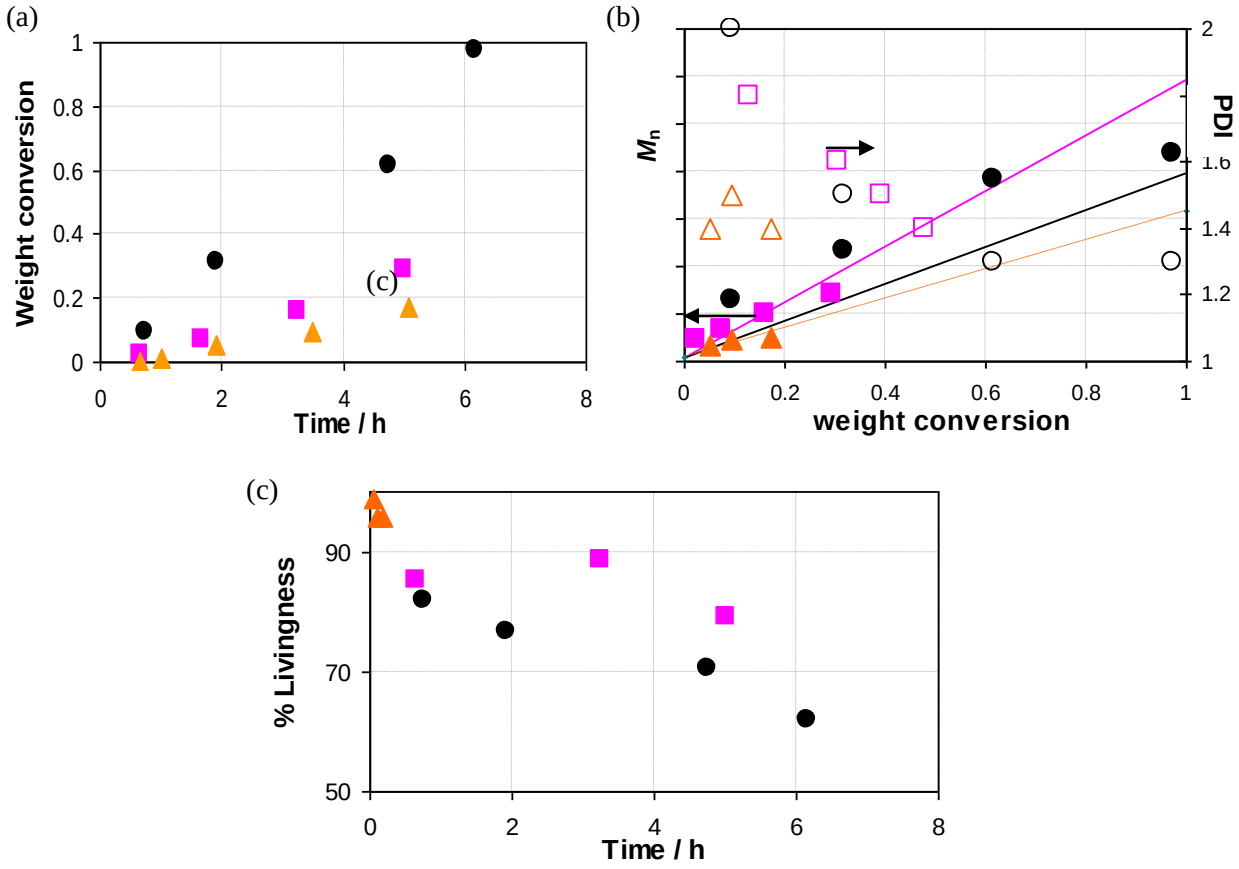

Figure 12. Polymerizations of (W1)

▲(BCP 38, 12% free SG1, M_n (x = 1) = 0.8 AU), ■ (BCP 39, M_n (x = 1) = 1.5 AU) and ● (BCP 39, M_n (x = 1) = 1.5 AU) (a) Overall weight conversion obtained by HPLC vs time; (b) M_n (full symbols) and PDI = M_w/M_n (corresponding empty symbols) with a solid and dashed lines for M_n^{theo} values and (c) overall percentage of SG1-terminated chains vs time.

5.1.2.2. First Block: P(E-co-W1) in DMSO

Monomer E was introduced as a co-monomer in the first hydrophilic block for several reasons: i) to improve livingness; ii) to decrease the hydrophilic character, which led to instability of the film in water and iii) to give some flexibility to the film for improved comfort.

5.1.2.2.1. Variation of Initiator Concentration

Copolymerizations of E were run in DMSO at 100–120 °C in a 100-mL glass reactor, Table 6. Reactions were initiated by BlocBuilder® MA. During adjustment of experimental conditions W1 concentration was locked at 24 wt % and the initiator concentration was decreased.

Table 6. Route 2 to First Block: P(E-co-W1); Variation of Initiator Concentration

Expt.	$[E]_0$ mol/L	W1 wt%	Conversion[a)] %
BCP 32	1.6	24	79
BCP 65	1.6	24	81
BCP 66	1.7	26	83
BCP 67	1.6	24	83

[a)] weight global conversion calculated obtained by GC and HPLC.

The global conversion evolutions were close for these experiments, Figure 13. The initiator concentration did not affect conversion. All copolymerizations were performed in 100-mL glass reactors. Several problems appeared when this copolymerization was started in a 2-L pressure reactor. In fact, the global conversion evolution was lower (after 4 h, global conversion of BCP 77 was close to 15%).

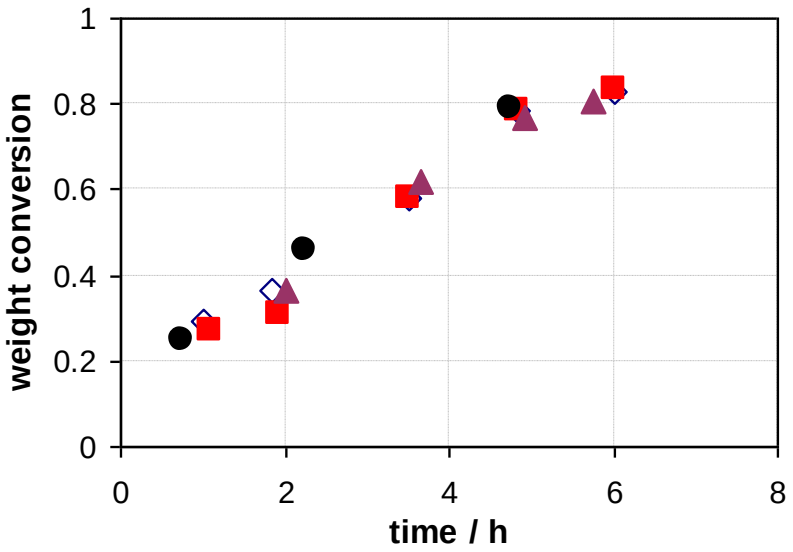

Figure 13. Overall Weight Conversion

● (BCP 32, M_n (x = 1) = 0.55 AU), ▲ (BCP 65, M_n (x = 1) = 1 AU), ■ (BCP 66, M_n (x = 1) = 1.7 AU) and ◊ (BCP 67, M_n (x = 1) = 2.6 AU).

5.1.2.2.2. Summary of the First Block to be Used in a Second Step

All hydrophilic first-block copolymers made for subsequent copolymerization to P(A) are summarized in Table 7. The global weight conversions were high, 60–85%. The number-average molar mass and composition of each first block are summarized in Table 8.

Table 7. Route 2—First Block: P(E-co-W1) to Be Used in Second Step

Expt.	$[E]_0$ mol/L	W1 wt%	Conversion[a)] %
BCP 81	1.6	24	56
BCP 99	1.6	24	87
BCP 114	1.1	50	71
BCP 123	1.2	50	70

[a)] weight global conversion calculated obtained by GC and HPLC.

Table 8. Copolymerizations of E with W1

Expt.	$[E]_0$ mol/L	W1 wt%	*t* h	Conversion[a)] %	M_n[theo b)] AU	M_n[exp c)] AU	PDI	Composition [d)] mol%
BCP 81	1.6	24	5.2	56	1.45	1.2	1.8	75 E – 25 W1
BCP 99	1.6	24	4.2	87	2.3	2.2	1.4	80 E – 20 W1
BCP 114	1.1	50	4.2	71	1.1	1.4	1.3	*49 E – 51 W1
BCP 123	1.2	50	4.6	73	1.7	2.0	1.3	*51 E – 49 W1

[a)] Weight global conversion calculated obtained by GC and HPLC.
[b)] Theoretical M_n calculated at experimental conversion.
[c)] Experimental M_n obtained by SEC in DMSO with $NaNO_3$ with a PW1 conventional calibration.
[d)] Experimental composition of block copolymer obtained by ^{13}C NMR in d_6-DMSO or for * with the individual conversion.

5.1.2.3. Diblock: P(E-co-W1)-b-P(A)

The first block copolymer solutions of P(E-co-W1)-SG1 were used to initiate attachment of the second block, P(A). All macroinitiator solutions were stripped to remove excess residual monomers, as their presence can impact the micro-phase segregation of the diblock copolymer. The impact of the molecular weight, the W1 concentration, the ratio between the first and the second block were studied.

5.1.2.3.1 P(E-W1)-*b*-PA, M_n = 1.25

Polymerizations of A in DMSO at 110–120 °C were initiated by a macroinitiator solution of P($E_{75\%}$-co-W1)-SG1 (BCP 81). This first block contained 25% of W1 and had M_w = 1.25 AU. The macroinitiator concentration was varied as shown in Table 9.

Table 9. Route 2—Diblock: P(E-co-W1)-b-P(A); M_n = 1.25 AU

Expt.	[First block]$_0$ mol/L	$[A]_0$ mol/L	ratio [a)] first/second block	Conversion[b)] %
BCP 85	1.7×10^{-3}	1.8	1.2 / 5.5	47
BCP 89	1.4×10^{-3}	1.7	1.2 / 6.6	45

[a)] Theoretical ratio between the first block and the second block (if it will reach 100% of conversion).
[b)] Weight global conversion calculated obtained by GC and HPLC.

Homopolymerizations of A were not controlled because no co-monomer was added. Residual quantities of E seemed to be too low for effective control and high conversion, Figure 14 (a). Nevertheless, the molecular weight values were close to the theoretical values, Figure 14 (b).

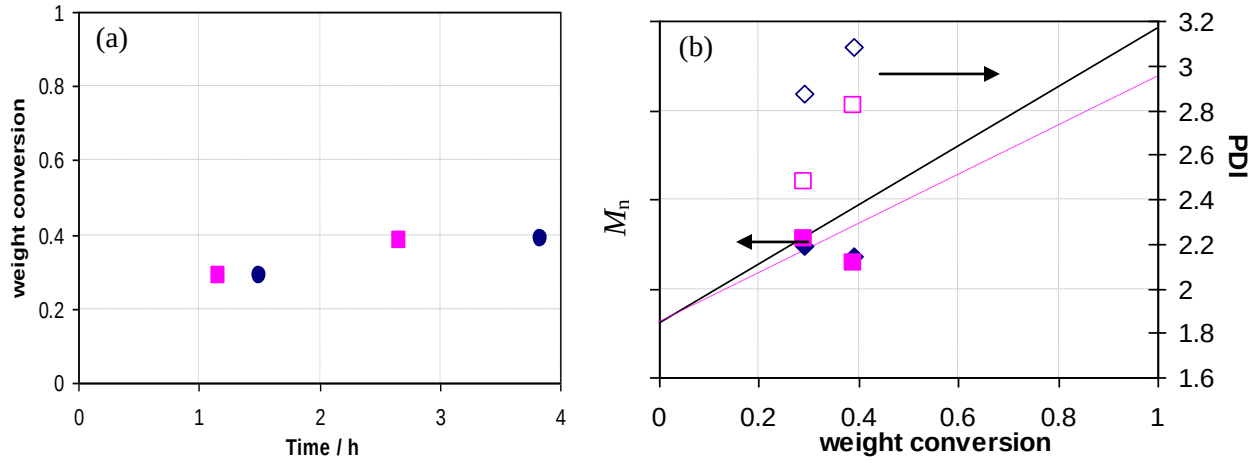

Figure 14. Polymerizations of A onto P(E-co-W1)
■ (BCP 85, $M_n^{theo}(x = 1) = 6.8$) and ● (BCP 89, $M_n^{theo}(x = 1) = 7.9$) (a) Overall weight conversion obtained by GC and HPLC vs time and (b) M_n (full symbols) and PDI = M_w/M_n (corresponding empty symbols) with a dashed line and a solid line for M_n^{theo} values.

5.1.2.3.2 P(E-co-W1)-b-P(A), M_n = 2.25 AU

Polymerization of A in DMSO at 110–120 °C was initiated by macroinitiator solution P(E-co-W1)-SG1 (BCP 99), Table 10. The first block contained 20% W1 and had M_w = 2.25 AU.

Table 10. Route 2—Diblock: P(E-co-W1)-b-P(A); M_n = 2.25 AU

Expt	[First block]$_0$ mol/L	[A]$_0$ mol/L	First/second block ratio[a]	Conversion[b] %	M_n^{theo}[c] AU	M_n^{exp}[d] AU	PDI	%W1[e] mol%
BCP 102	2.9×10^{-3}	1.1	2.3 / 1.9	40	3	3.1	1.5	14

[a] Theoretical ratio between the first block and the second block (if it will reach 100% of conversion).
[b] Weight global conversion calculated obtained by GC and HPLC.
[c] Theoretical M_n calculated at experimental conversion.
[d] Experimental M_n obtained by SEC in DMSO with $NaNO_3$ with PW1 conventional calibration.
[e] Percentage molar of W1 in all-diblock copolymer determined by ^{13}C NMR.

These polymerization results were similar to the two previous polymerizations (BCP 85 and BCP 89). The greater length of the first block did not impact the polymerization.

5.1.2.3.3 P($E_{51\%}$-co-W1)-b-P(A), M_n = 2 AU

Polymerizations of A in DMSO at 110–120 °C were initiated by a macroinitiator solution P($E_{51\%}$-co-W1)-SG1 (BCP 123). The first block used contained 51% of W1 and had M_w = 2 AU. The concentration of macroinitiator was varied as shown in Table 11.

The evolution of the global weight conversion was slow and the concentration of the macroinitiator solution had a significant impact on the control of the molar mass, Figure 15.

Table 11. Route 2 – Diblock: P(E-co-W1)-b-P(A); M_n = 2 AU

Expt.	[First block]$_0$ mol/L	[A]$_0$ mol/L	ratio [a] first/second block	Conversion[b] %
BCP 127	1.0×10^{-3}	2.0	2 / 10.3	44
BCP 128	1.7×10^{-3}	1.5	2 / 4.5	46
BCP 143	3.1×10^{-3}	0.5	2 / 1.2	63

[a] Theoretical ratio between the first block and the second block (if it reached 100% conversion).
[b] Weight global conversion calculated from GC and HPLC data.

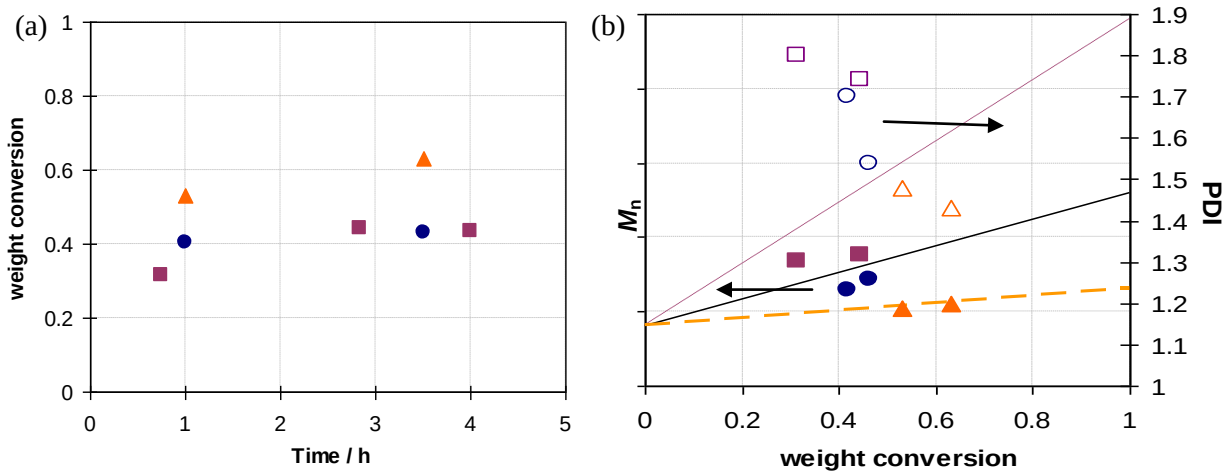

Figure 15. Polymerizations of A
■ (BCP 127, $M_n^{theo}(x = 1)$ = 12.3 AU), ● (BCP 128, $M_n^{theo}(x = 1)$ = 6.5 AU) and ▲ (BCP 143, $M_n^{theo}(x = 1)$ = 3.3 AU) (a) Overall weight conversion obtained by GC and HPLC vs time and (b) M_n (full symbols) and PDI = M_w/M_n (corresponding empty symbols) with dashed and solid lines for M_n^{theo} values.

5.1.3. Route 3: P(E-co-W2)-b-P(A)

In this route, a new hydrophilic monomer was tested. W2 was chosen because of its established performance in membranes for water filtration. For these copolymers, the effect of the ratio between the first and the second block and also the effect of the concentration in W2 was investigated. Monomer E was used as a co-monomer of W2 in the first block for the same reasons as in the second route.

5.1.3.1. First Block: P(E-co-W2)

Copolymerizations of E with a certain amount of W2 (20 and 35 wt%) were done in bulk. The concentration of BlockBuilder® MA was varied. The temperature in the reactor and the control of exotherm at the beginning of these reactions had a significant impact on the control of these copolymerizations.

5.1.3.1.1. Impact of Temperature

The impact of the temperature ramp at the beginning of this reaction was studied. These copolymerizations were done in bulk at 90–110˚C, Table 12.

Table 12. Route 3—First Block: P(E-co-W2); Impact of Temperature

Expt.	$[E]_0$ mol/L	Conversion[a] %	Temperature ramp (Time to reach 90 °C)	(Time to reach 100 °C)
BCP 150	5.8	58	36 min	3 h 10 min
BCP 152	5.8	56	20 min	2 h 30 min
BCP 154	5.8	81	8 min	18 min

[a] weight global conversion calculated from GC and HPLC data.

For two reactions (BCP 150 and BCP 152), the evolution of the weight conversion was low and the temperature ramp was slow at the beginning. At the end of these reactions, the mixtures were dark yellow, indicative of a high concentration of free nitroxide.

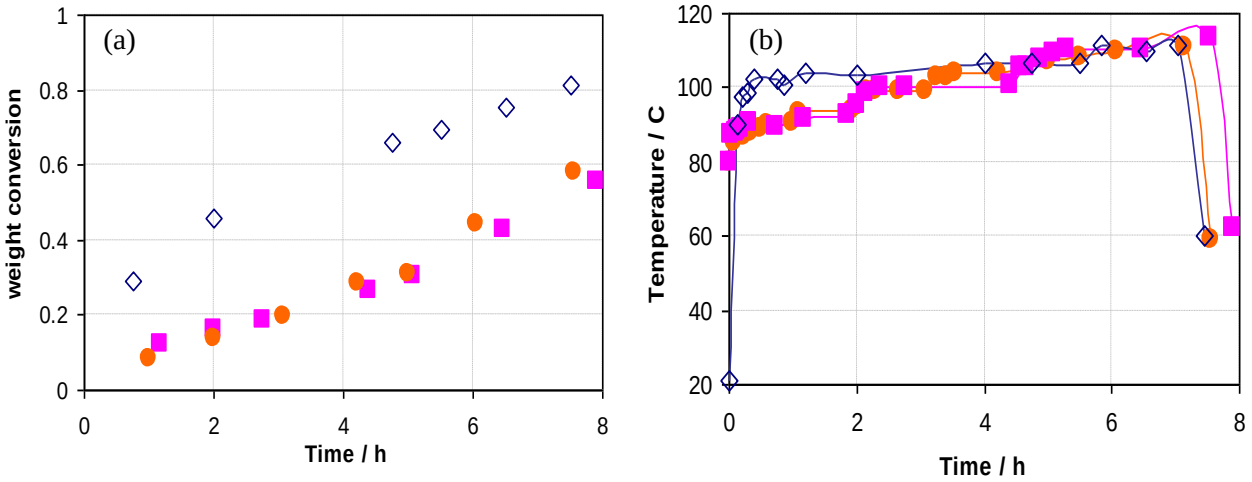

Figure 16. Copolymerizations of E
● (BCP 150), ■ (BCP 152) and ◊ (BCP 154) (a) Overall weight conversion obtained by GC vs time; (b) evolution of the temperature in the reactor mixture

With these conditions, it seems that the initial temperature was too low, which triggered the formation and accumulation of free nitroxide in the media. This high concentration slowed down the copolymerization. Increasing the temperature at the beginning of the reaction increased the rate of copolymerization and the final conversion value.

5.1.3.2. Diblock: P(E-co-W2)-b-P(A)

All polymerizations of A were done in toluene at 110–125 °C using different first block macroinitiator solutions of P(E-co-W2)-SG1 at different concentrations, Table 13.

In this polymerization, the residual concentration of E was very high. This high concentration permitted better control of the polymerization of A. In all cases, the final weight conversion was high. Molar masses were not controlled and M_n values were close to targets.

Table 13. Route 3—Diblock: P(E-co-W2)-b-P(A)

Expt.	First Block	[First block]$_0$ mol/L	[A]$_0$ mol/L	ratio[a] first/second block	Conversion[b] %
BCP 153	BCP 151	1.4×10^{-2}	0.8	24 / 11	72
BCP 155	BCP 154	1.5×10^{-2}	2.7	15.5 / 21	50
BCP 166	BCP 162	1.4×10^{-3}	1.6	22 / 12	40
BCP 167	BCP 165	1.9×10^{-3}	3.9	8 / 22.5	55

[a] theoretical ratio between the first block and the second block (if it will reach 100% of conversion)
[b] weight global conversion calculated obtained by GC and HPLC.

5.2. Block Copolymer Characterization

5.2.1. P(A-co-B)-b-(W1) Family

In this first family of BCPs, P(A-co-B)-b-(W1), the first hydrophobic block was a combination of two monomers, A and B. The second block consisted of a hydrophilic W1 chain. One exception was BCP 112, in which the co-monomer E was added to the hydrophilic block.

Figure 17 presents a summary of all BCPs synthesized in the family of P(A-co-B)-b-P(W1). It is important to note that the first block is a statistical distribution of A and B. The intent of the bar chart is only to indicate the ratio between A and B. The red stars indicate WVTR above the target of 1,000 g/m²/day. The black cross indicates that it was impossible to cast films in a blend with K1 (see next section, BCP blends).

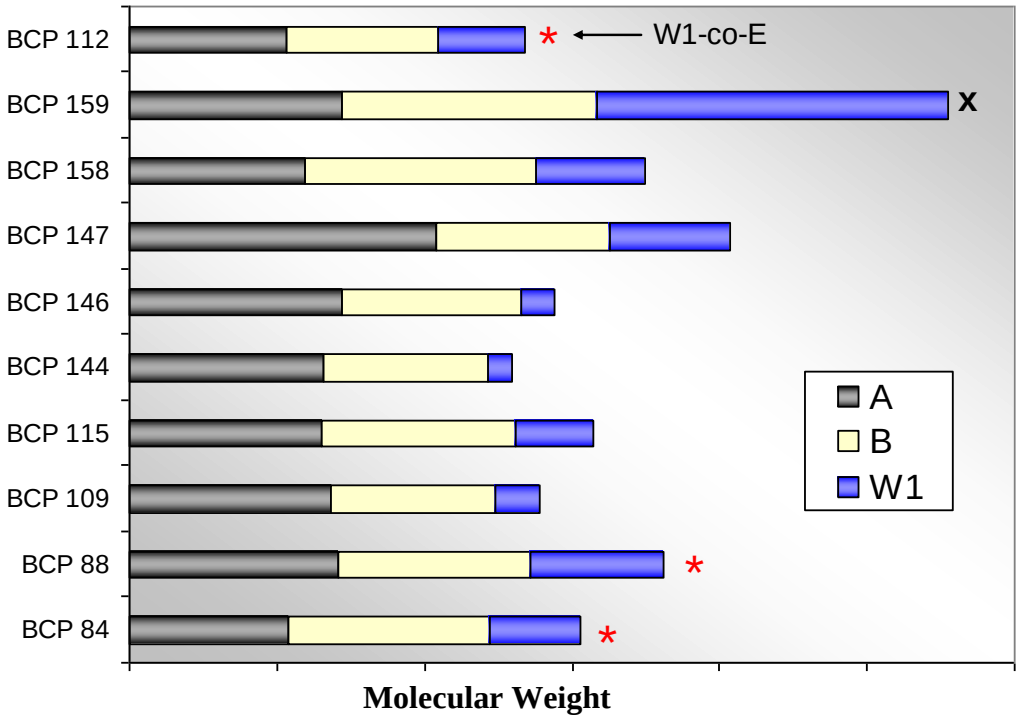

Figure 17. BCPs Synthesized of the Family P(A-co-B)-b-P(W1)

5.2.1.1. Coating and Film Integrity

All solutions were degassed under vacuum at room temperature and coated on aluminum foil at 155 °C for 10 min. Films were released from their aluminum support by immersion in deionized water, then allowed to dry at room temperature overnight.

Table 14. Diblock Copolymers Summary and Films Characterization.

Expt.	First block	M_n^{first}/M_n^{second} a) AU	M_n diblock AU	%W1 b) mol%	Film aspect
BCP 84	BCP 82	1.5 / 2.5	3.1	20	Lost integrity (Partially soluble)
BCP 88	BCP 82	1.5 / 1.9	3.6	25	Lost integrity (Partially soluble)
BCP 109	BCP 104	1.4 / 1.1	2.8	11	Kept integrity
BCP 115	BCP 104	1.4 / 2.2	3.1	17	Swelling, lost integrity
BCP 144	BCP 124	1.8 / 0.7	2.6	6	Kept integrity
BCP 146	BCP 124	1.8 / 0.9	2.9	8	Kept integrity
BCP 147	BCP 124	1.8 / 2.2	3.4	24	Kept integrity
BCP 158	BCP 154	2.5 / 3.8	3.5	21	Swelling, lost integrity
BCP 159	BCP 154	2.5 / 8.8	5.6	43.5	Lost integrity (hydrogel)
BCP 110	BCP 104	1.4 / 1.5	2.7	-	Kept integrity
BCP 112	BCP 104	1.4 / 1.9	2.7	9	Kept integrity

a) Number-average molar ratio of the first block (determined by SEC) and the second block (if it reached 100% conversion)

b) Percentage molar of W1 in all diblock copolymer determined by ^{13}C NMR.

BCP with high contents of W1 lost their integrity after immersion in water, and BCP molecular weight also seemed to have an impact. These results show the importance of W1 content and distribution as well as molecular weight.

5.2.1.2. WVTR Results

Water transmission was successfully measured for only three of the Route 1 samples. Although additional films retained integrity in water, their mechanical properties were too poor for them to be handles without damage. Many films could not be mounted on the aluminum support or survive the WVTR test, Figure 18.

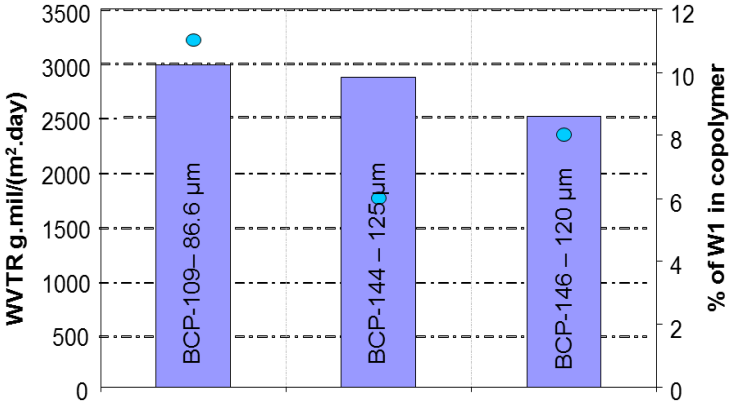

Figure 18. WVTR of Neat BCP Films

■ Mocon values at 37.8 °C, RH 10 ~ 100% and (●) percentage of W1 in the diblock copolymer

These high WVTR values can be explained by the high content of W1. This first route resulted in the synthesis of eleven diblock copolymers, each of which was evaluated in blends.

5.2.2. P(W1-co-E)-b-P(A) Family

Figure 19 is a summary of all BCPs synthesized in the P(W1-co-E)-b-P(A) family. The first block is a statistical distribution of W1 and E. The intent of the bar chart is only to indicate the ratio between W1 and E. The red stars indicate WVTRs above the target value of 1 kg/m²/day. The black cross indicates that it was impossible to manufacture films in a blend with K1.

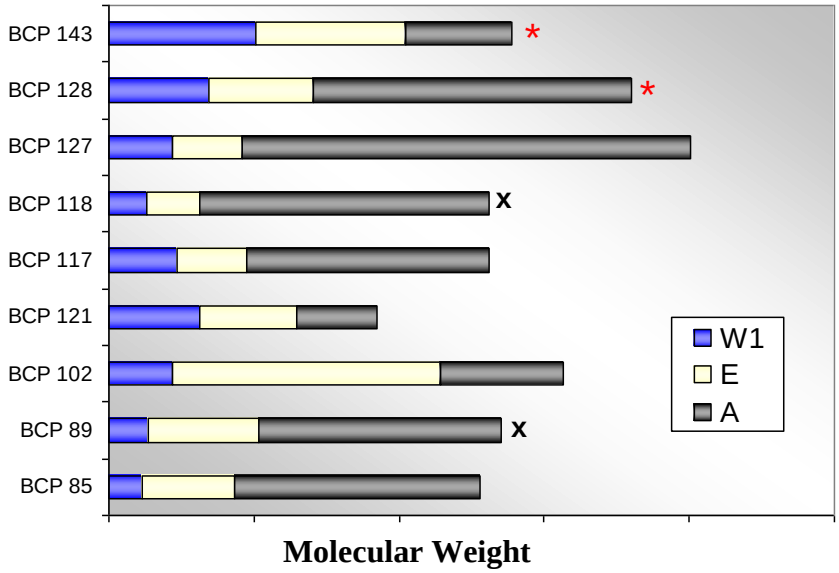

Figure 19. BCP Synthesized of the Family P(W1-co-E)-b-P(A)

5.2.2.1. Coating and Film Integrity

Table 15 presents a summary of the BCP and film characterization. Several BCP films lost integrity after immersion in water, confirming the need for blending with a host polymer.

Table 15. Diblock Copolymer Summary and Film Characterizations.

Expt.	First block	M_n^{first} / M_n^{second} a) AU	M_n diblock AU	%W1 c) mol%	Film aspect
BCP 85	BCP 81	1.25 / 5.5	2.6	9	Kept integrity
BCP 89	BCP 81	1.25 / 6.6	2.7	10	Kept integrity
BCP 102	BCP 99	2.25 / 1.9	3.1	14	Lost integrity (partially soluble)
BCP 121	BCP 114	1.4 / 0.9	1.8	34	Lost integrity (partially soluble)
BCP 117	BCP 114	1.4 / 3.35	2.6	18	Kept integrity
BCP 118	BCP 114	1.4 / 7.9	2.6	10	Kept integrity
BCP 127	BCP 123	2 / 10.3	4	11	Kept integrity
BCP 128	BCP 123	2 / 4.45	3.6	19	Kept integrity
BCP 143	BCP 123	2 / 1.2	2.8	36	Lost integrity (partially soluble)

a) M_n of the first block (determined by SEC) and the second block (if it reached 100% of conversion).
b) Experimental M_n obtained by SEC in DMSO with $NaNO_3$ with a PW1 conventional calibration.
c) Percentage molar of W1 in all the diblock copolymer determined by ^{13}C NMR.

5.2.2.2. WVTR results

Several films analyzed with the Mocon apparatus are shown in Figure 20.

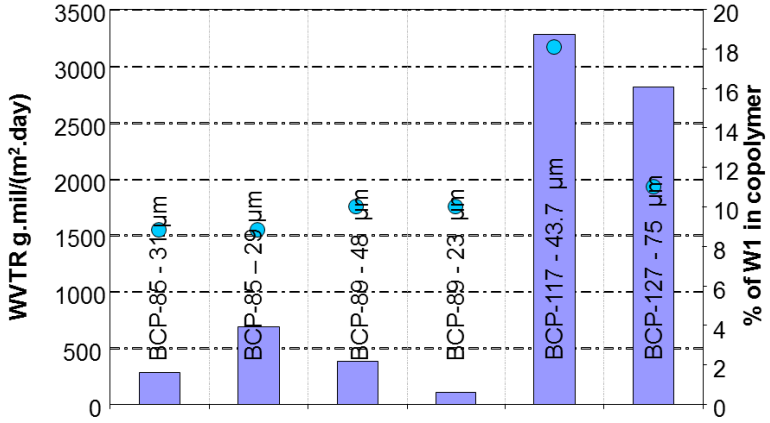

Figure 20. WVTR of Neat BCP Films

■ Mocon values at 37.8 °C, RH 10 ~ 100% and (●) percentage of W1 in diblock copolymers

The superposition of WVTR values and percentage of W1 in the diblock copolymer suggested a link between these two data sets, Figure 20. The higher the concentration of W1, the higher the WVTR value. Thickness had an impact as well. Moreover, WVTR value varied across the film.

In this part, several diblock copolymer of P(BA-co-W1)-b-(PA) were synthesized in DMSO and coated on aluminum substrate. The mechanical properties were high enough to allow analysis of the WVTR through these films. The first result showed a correlation between the WVTR value and the concentration of W1 in the diblock copolymer.

5.2.3. P(W2-co-E)-b-P(A) Family

The last family of BCPs was very similar to the second one but the hydrophilic monomer W2 was substituted for W1 to produce different characteristics. Figure 21 summarizes all BCPs synthesized in the P(W2-co-E)-b-P(A) family. The first block is a statistical distribution of W2 and E. The intent of the bar chart is only to indicate the ratio between W2 and E.

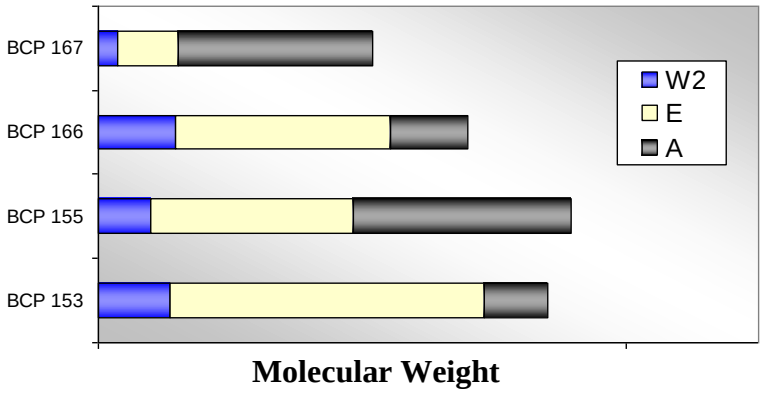

Figure 21. BCPs Synthesized of the Family P(W2-co-E)-b-P(A)

5.2.3.1. Coating and Film Integrity

The solutions were dried under vacuum at 110 °C for 3 h to remove any residual toluene or monomers. Nevertheless, none of the films could be analyzed. For BCP 155 and 167, the A content was too high and the films were too brittle. For the two other copolymers, the films were too tacky (high content of E).

5.3. Summary

Three kinds of BCPs were synthesized with different monomers and ratios between each monomer and each block. To improve permeability and mechanical and thermal properties of these membranes, a majority of these BCPs will need be used in a blend with other polymers.

6. BLOCK COPOLYMER BLEND PREPARATION AND CHARACTERIZATION

Host K1 was dissolved in NMP and then mixed with the BCP/DMSO solution. The resulting mixture was, stirred at 60 °C for 2–3 h. This route was found to be the easiest to manufacture good quality films.

Several problemss appeared when using DMSO, such as gel formation, low solids content, or high viscosity, and this route was abandoned at Arkema. University of Cincinnati had some success and decided to pursue this route. It turned out that following both approaches in parallel was very beneficial for the overall understanding of the phenomena occurring during coating processes (nanostructuration and resulting impact on performance of the films).

6.1.1. P(A-co-B)-b-P(W1) BCP

6.1.1.1. Different BCP with the Same BCP/host Ratio

BCP 84 and BCP 88 were mixed with a K1 solution in NMP. The ratio between the BCP and K1 was varied, Figure 22.

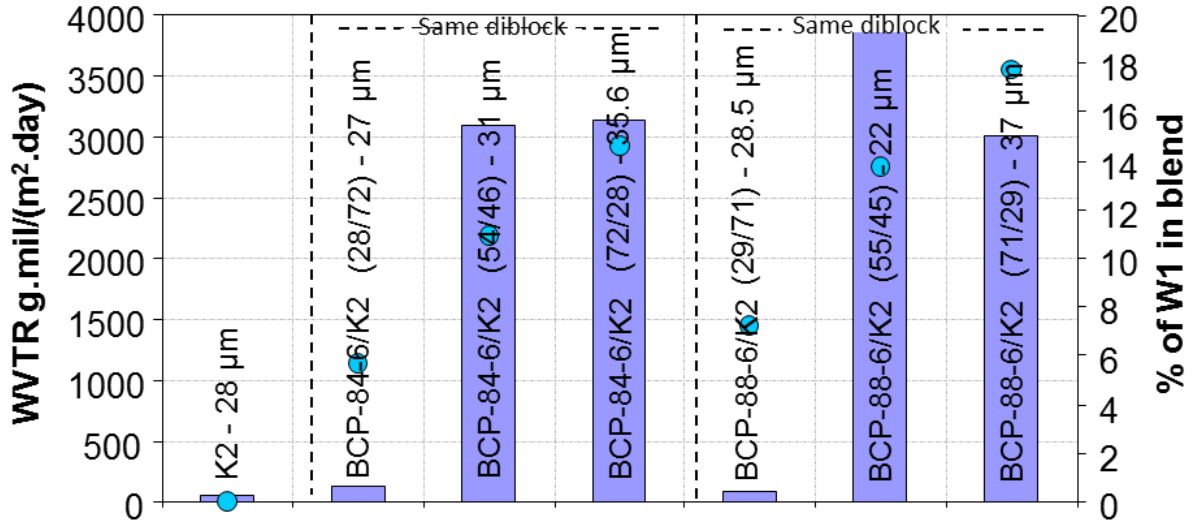

Figure 22. WVTR of Different BCPs in Blend with K1 in NMP

■ Mocon values at 37.8 °C, RH 10 ~ 100% and (●) percentage of W1

When the concentration in BCP was too low (around 30 wt%), no improvement in the film breathability was observed, Figure 22. A minimal amount of BCP was necessary to reach WVTR values above 1 kg/m^2/day. After a critical amount of BCP, WVTR values reached a plateau. This effect may be linked to the morphology of the micro-phase separation of the BCP.

6.1.1.2. Variation of BCP/host Ratio with the Same BCP

With this series of experiments the concentration of W1 seemed to have an impact on the WVTR result, Figure 23. After a certain amount of W1, the values were above the targeted value.

6.1.2. P(E-co-W1)-b-P(A) BCP

The BCP / K1 ratio was varied in Figure 24 (a) and set close to 50/50 in Figure 24 (b).

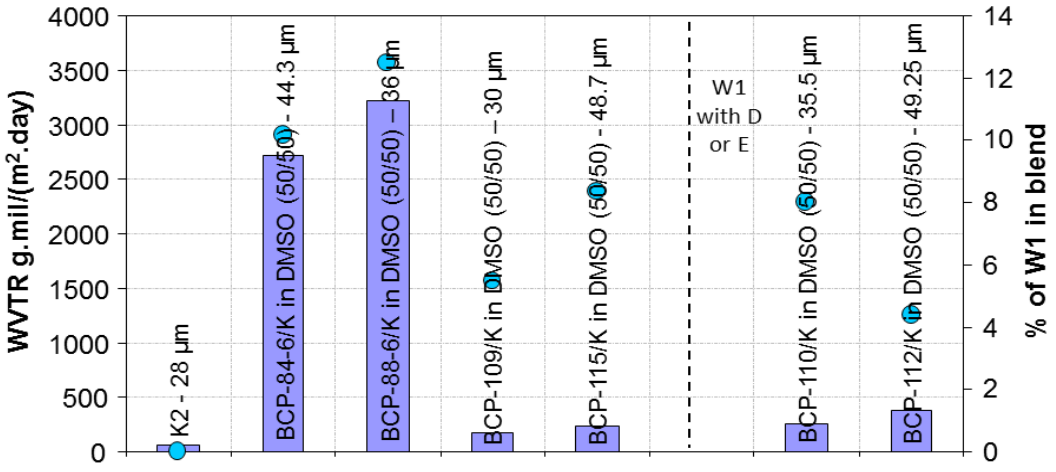

Figure 23.WVTR of BCPs in Blend with K1 in DMSO

■ Mocon values at 37.8 °C, relative humidity between 10 ~ 100% and (●) percentage of W1

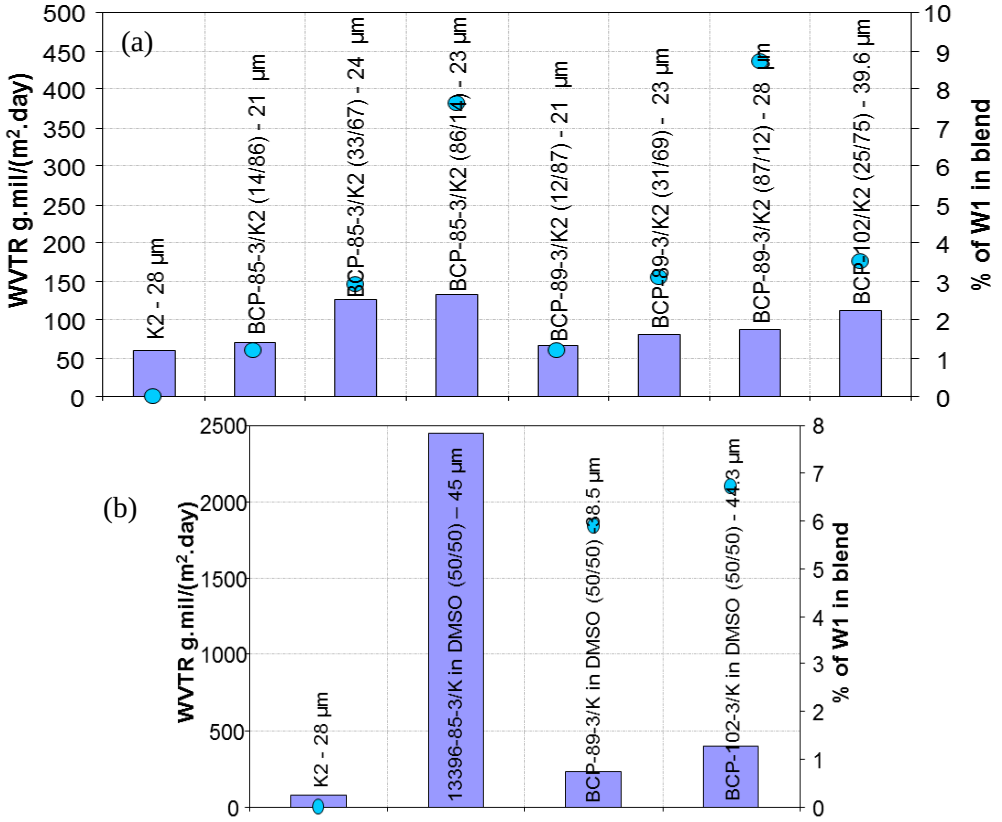

Figure 24. WVTR of BCP Blends with K1 in NMP or DMSO

■ Mocon values at 37.8 °C, RH = 10 ~ 100% and (●) percentage of W1 (a) on the blend of BCP with K1 in NMP and (b) on the blend of BCP with K1 in DMSO

Figure 24 (a), shows low WVTR values, probably due to the low W1 concentration in the BCPs. The same blends made in DMSO, Figure 24 (b), showed higher values.

6.1.3. Summary of BCP Blend WVTRs

Figures 25 and 26 document body-temperature WVTR (not normalized for thickness) and permeability (normalized) obtained at Arkema on most of the BCPs synthesized, in a blend with K1 at four loadings, i.e., 40%, 50%, 62.5% and 75%. As expected, WVTR values were higher than observed at UC at room temperature.

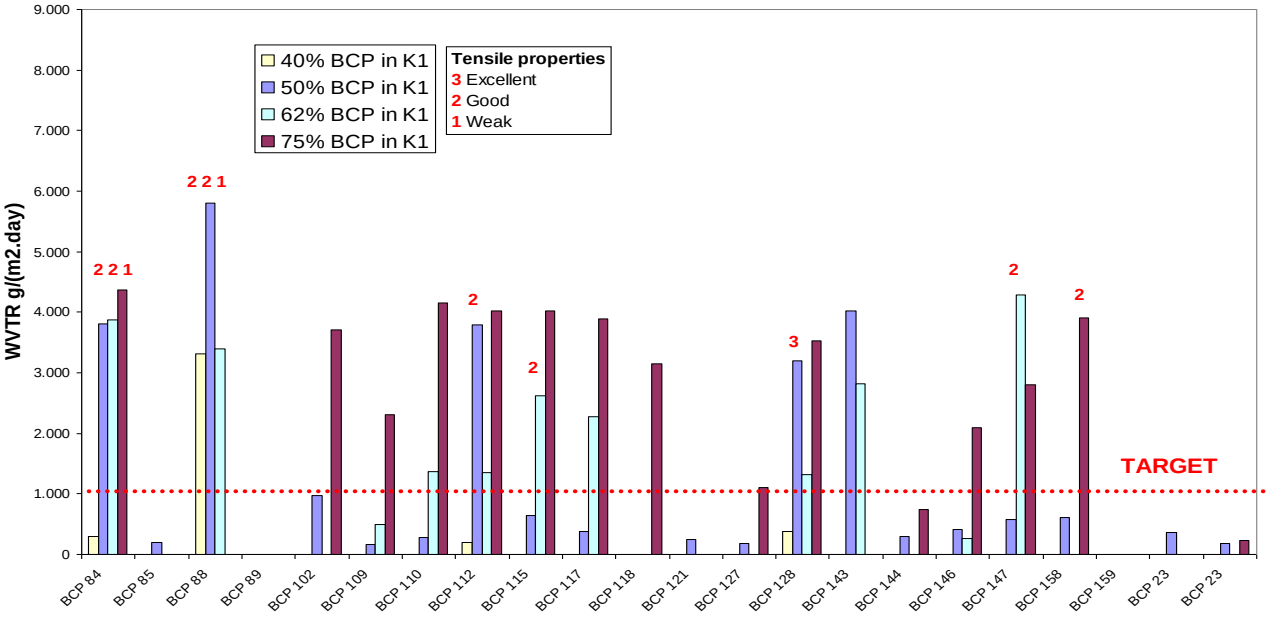

Figure 25. Body-temperature WVTR (Not Normalized for Thickness) of BCP Blended with K1 at Four Loadings

Red numbers, representing tensile strength, are indicated only for high-performance films (showing a combination of high WVTR and strength)

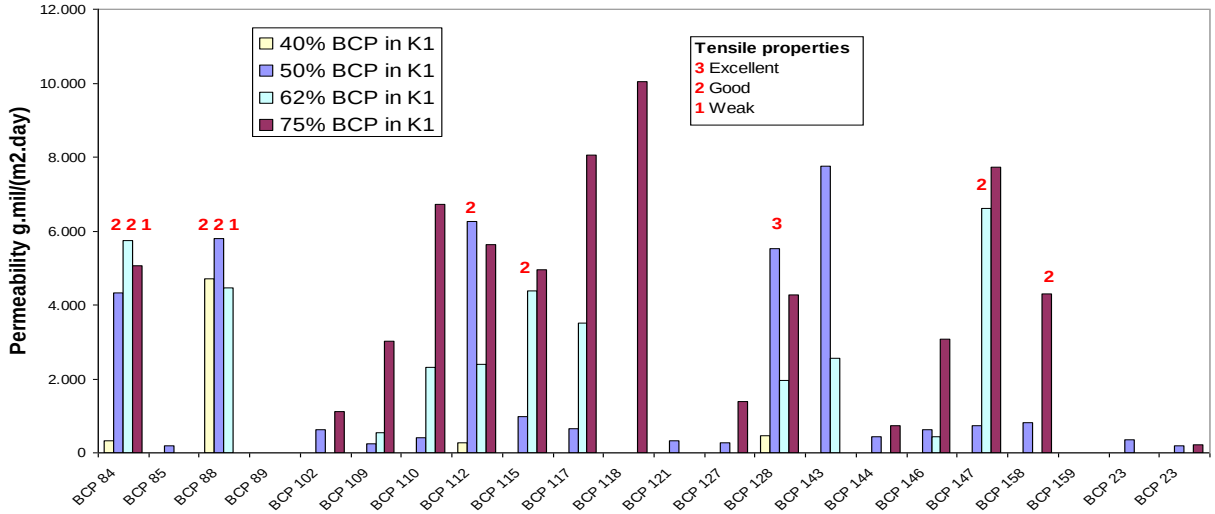

Figure 26. Body-Temperature Permeability (Normalized for Thickness) of BCP Blended with K1 at Four Loadings

Red numbers, representing tensile strength, are indicated only for high-performance films (showing a combination of high WVTR and strength).

The first observation is that the WVTR of a majority of blends was at or above the target value of 1 kg/m^2/day. In addition, a loading of 75% BCP in the blend gave slightly higher WVTR values than lower loadings. However, membranes of the latter showed higher chemical resistance and better mechanical strength. Blends that have a higher chance of success (identified in chart below with red numbers) are those that show high WVTR at or below 62.5% of BCP.

6.1.4. Evaluation of Mechanical Properties on BCP Blend Films

A score for mechanical properties was given to the different films (from 0, the lowest, to 3, the best). Figure 27 presents the tensile strength of the films according to their BCP content.

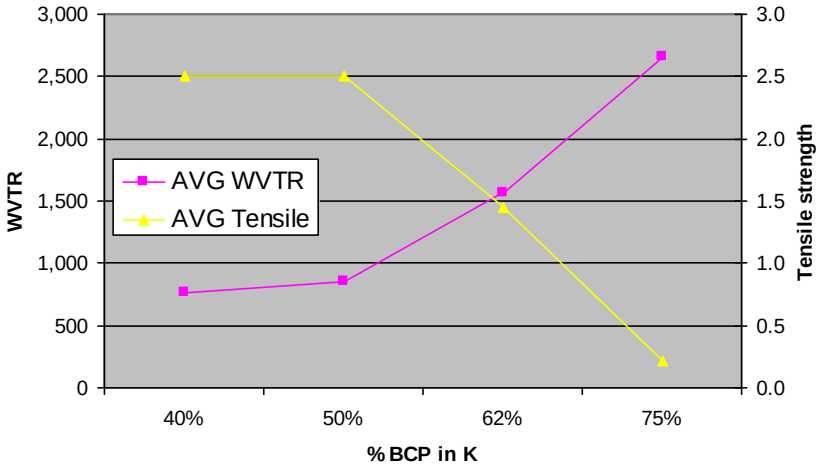

Figure 27. Tensile Strength Evaluation

Note: For the tensile strength, 0 is the lowest score.

When the % BCP in K1 was increased, membranes had a higher WVTR (better breathability) but they were more brittle.

6.1.5. Effect of Temperature on WVTR

WVTR of the best-performing films was measured at different temperatures, to assess the breathability of the films. Four temperatures were selected: 10, 23, 38 and 45 °C (Figures 28–30)

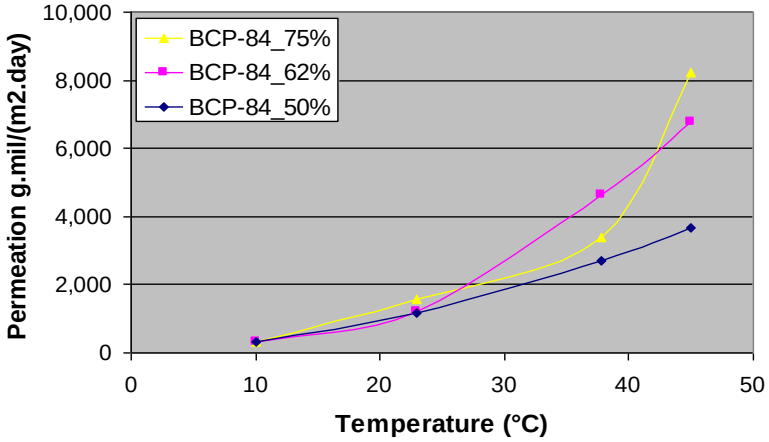

Figure 28. Permeation vs Temperature of BCP 84 at Different K1 Loadings

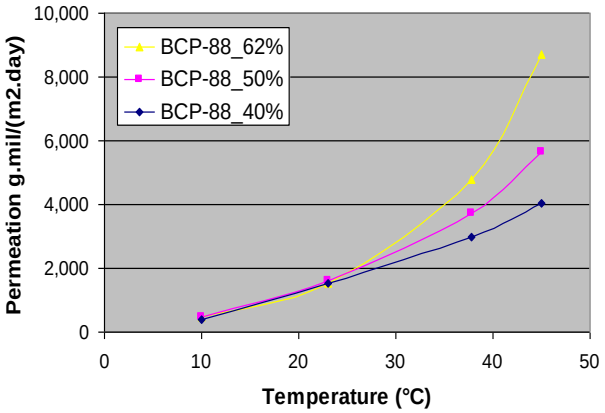

Figure 29. Permeation vs. Temperature of BCP 88 at Different K1 Loadings

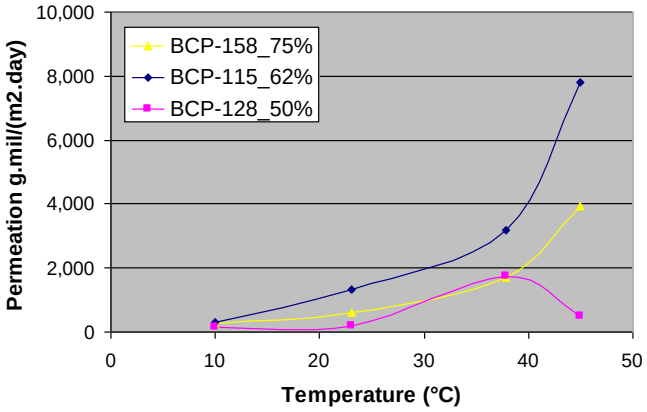

Figure 30. Permeation vs. Temperature of BCP 158, 115 and 128 (Different K1 Loadings)

Breathability is reported as permeation in g·mil/(m^2·day), where mil is a thickness unit that equals 25 µm. Whereas mil is a US unit, permeation expressed in g·mil/(m^2·day) is widely used in the industry. We are using it in this report because only permeation (which is the WVTR value normalized to the film's thickness), is a material-specific measure, that is independent of the film geometry. Performance expressed in permeation units is thus a material performance, not a film performance (see figures below). As expected, permeation increases with temperature. Interestingly, films containing lower amounts of BCP (about 50%) show a linear progression and films containing higher amounts of BCP (62 to 75%) show an exponential behavior.

It is also interesting to note that permeation values were up to 4 times higher at 45 °C than at room temperature, which is an important parameter for field operations.

6.1.6. Effect of the Host Matrix

In this section, we explore different grades of the host polymer. Host K1 was selected for its good balance of mechanical performance (flexibility) and barrier vs. chemical agents. We tried two other versions of K1 (K0 and K2) containing different amounts of additives to improve flexibility. Figure 31 shows that the nature of the host has little influence on the permeation. This

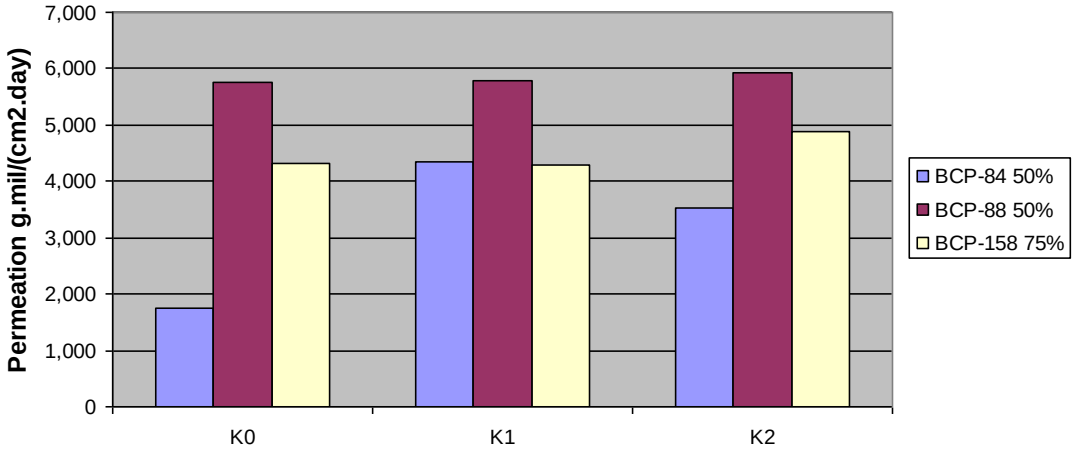

Figure 31. Permeation of BCP 84, 88 and 158 in three host polymers: K0, K1 and K2

result means that it was possible to maintain excellent levels of permeation while tuning stiffness or flexibility of the film.

6.2. Blend Preparation

6.2.1. Glassy Transition Temperature of Host Polymers N2 and N3

We measured the T_gs for host polymers N2 and N3 using DSC. Results show that T_g for N2 is in the range of 68 to 82 °C, slightly lower than that for N3 (71 to 89 °C). The degradation temperatures for N2 and N3 are 360 and 300 °C, respectively, suggesting thermal stability at our designated membrane casting temperatures (90 °C).

DSC and TGA results for N2 and N3 host polymers imply that the membrane casting temperature should be higher than 80 °C and lower than 300 °C.

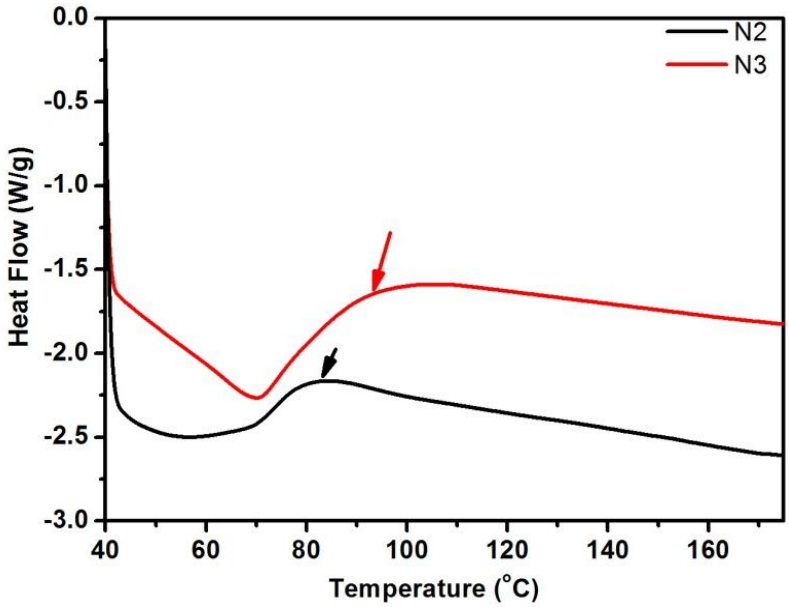

Figure 32. DSC and TGA Results for N2 and N3 Host Polymers

6.2.2. Determination of Host Polymers and Blending Ratios

K1 was selected due to its characteristic mechanical property enhancement on the N1/N2 based BCPs. We cast membranes with varied weight ratios and their morphology was studied as described below.

6.2.3. Domain Size by Neutron Scattering

We characterized BCP–K1 blends using SANS (section 3.3.2.8) which measured the in-plane structure of the membranes. These data were a critical input in modeling transport and optimizing BCP composition, blending ratio and processing protocol.

Figure 33 shows the change of the SANS profile with hydrophilic content in the BCP for 60/40 BCP/K1 blends (weight ratio). The peak is attributed to the periodic domain structure of the block copolymer. The shift in the peak position with composition implies that the domain

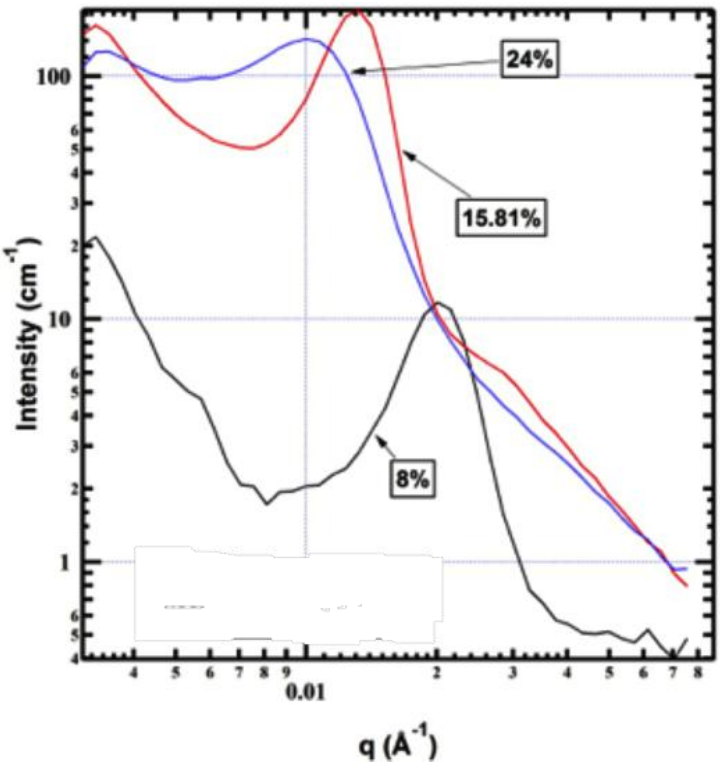

Figure 33. Evolution of the SANS Profile with mol% Hydrophilic Content of the BCP
The peak position is a measure of the domain spacing, ETA = $2\pi / q_{peak}$.

spacing increased with the hydrophilic content of the BCP. Figure 34 shows that the domain spacing roughly tracked water/DMMP selectivity.

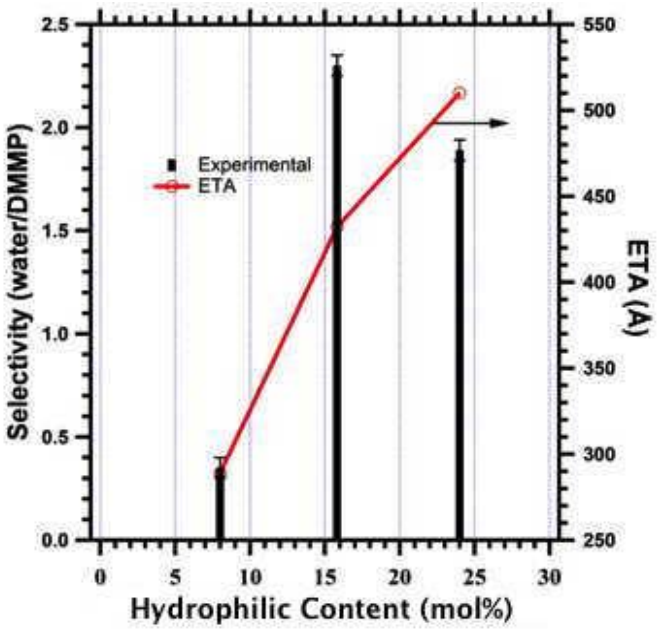

Figure 34. Relationship Between the Domain Spacing (ETA) and Membrane Selectivity as a Function of Hydrophilic Content in the BCP

Several samples were characterized dry and in the presence of heavy water (D_2O) vapor. Heavy water is used because it offers high neutron contrast to both components of the blend. Figure 35 shows the response to water vapor for two blends. For the 75/25 (wt%) BCP/K1 blend the increase in the peak intensity is because heavy water is going into the phase with lower initial neutron scattering length density (presumably the hydrophilic block of the BCP). For the sample with less BCP, the trend is reversed.

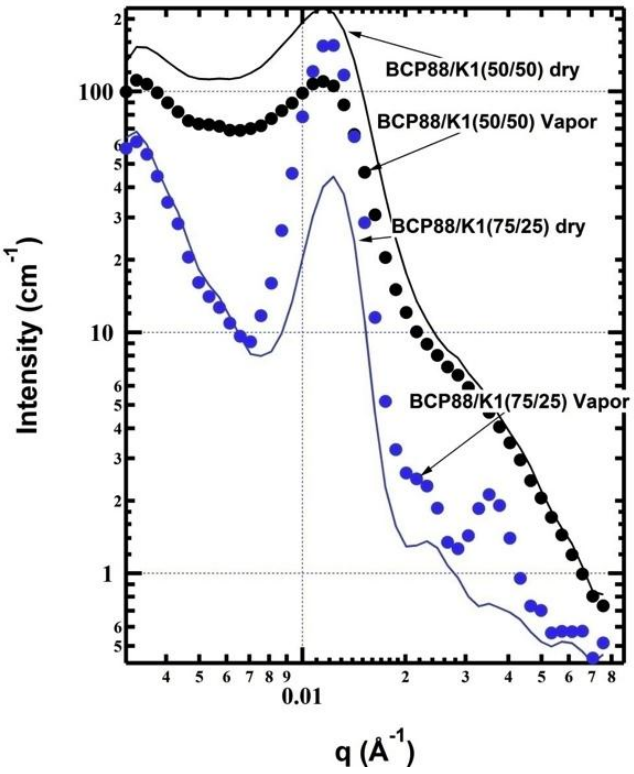

Figure 35. Change in SANS Profile of BCP/K1 Blends on Exposure to Heavy Water

The intensity of the peak increases for the blend containing 75 wt% BCP but decreases for the blend with 50 wt% BCP.

6.2.4. Interface Morphology by Neutron Reflectivity

BCP blend films were deposited on Si wafers and examined using neutron reflectivity. Based on the review of other related works, these appear to be the first experiments to determine the response of copolymer blends to water-vapor exposure.

Figures 36–38 show raw reflectivity data (left) and the corresponding scattering length density (SLD) profile (right). SLD depends on composition and density. If the films show phase separation normal to the substrate, the SLD profile would not be flat, as seen for the neat copolymer film in Figure 36. Thus pure K1 showed no bulk phase separation as expected for a one-component film. There is, however, a narrow region of reduced SLD right at the oxide interface, which may indicate reduced density due to contact with the high-energy oxide wafer surface.

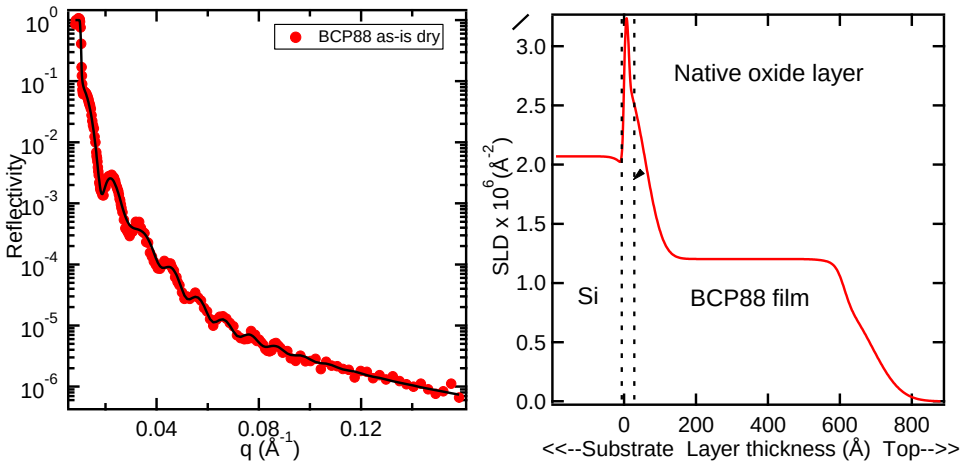

Figure 36. NR Data and SLD Profile for Pure BCP88

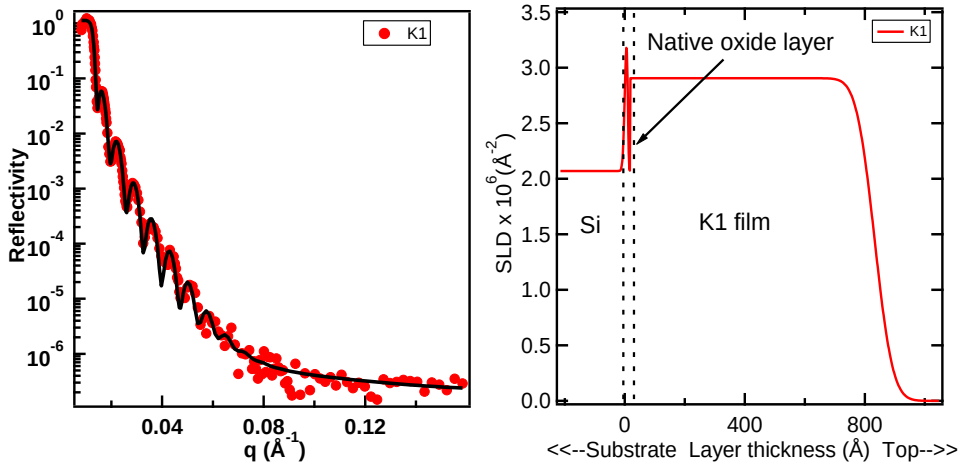

Figure 37. NR Data and SLD Profile for Pure K1

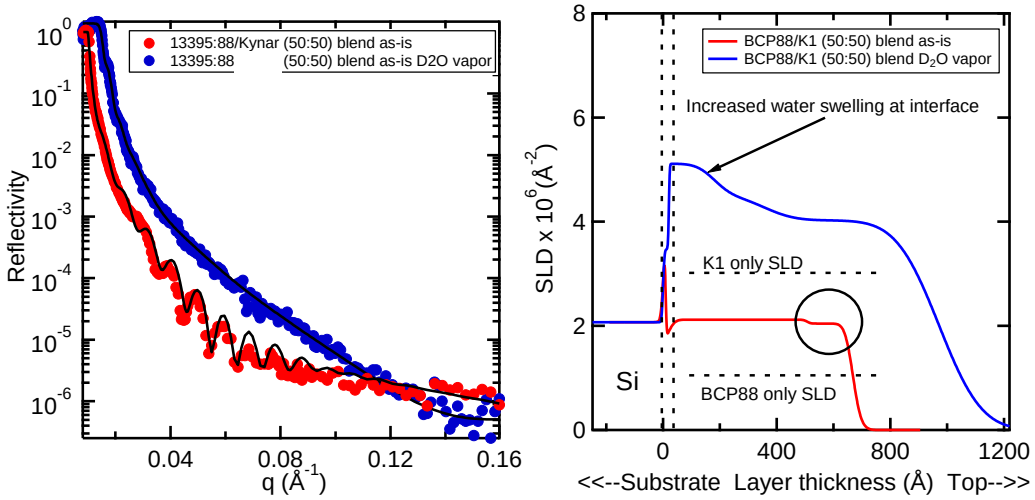

Figure 38. NR Data And SLD Profile For BCP88/K1 Blend in the Dry State and in the Presence of Saturated D_2O Vapor

Figure 38 shows a 50-50 K1–BCP88 blend dry and in the presence of D_2O vapor. The scattering length density of the dry-state blend falls midpoint between the SLD values expected for blended K1 and BCP88. Although there was a slight indication of phase separation at the air surface these data showed there is no layering of the domains in contact with the surface. This was a favorable result from the point of view of transport because layering would block vapor transport. The preferred structure was a continuous hydrophilic matrix extending from the wafer surface to the air surface, which seemed to be the case, at least for this blend ratio and BCP molecular weight ratio.

On exposure to D_2O (Figure 38), the film swelled by 40%. The increased SLD at the oxide interface showed that water favors this interface. From the measured SLD values the water content at the oxide interface was 64 vol%. Both the high degree of swelling and the non-uniform distribution of water in the film were unexpected based on the nearly uniform SLD profile observed in the dry state.

The increased water content at the oxide interface implies that in spite of the lack of out-of-plane phase separation, there was a distribution of hydrophilicity after exposure. It is possible that the film structure evolved upon absorption of water.

These films maintained their integrity in spite of high water content. The large water content should dramatically improve selectivity for water over simulants compared to what was predicted from the single-gas transport experiments. These results highlight the importance of mixed-gas experiments to judge the performance of the membranes in a realistic use scenario.

The air surface provided the only indication of out-of plane phase separation in the dry state.

6.3. Evaluation of Block Copolymers and Block Copolymer Blends

We measured the permeability of Arkema block copolymer blend membranes. Characterizations include permeation tests on chemical simulants including DMMP, tributyl phosphate (TBP) and methyl salicylate (MS) at room temperature, high temperature and co-feeding mixture settings.

To evaluate the permeability of the chemical simulants, the saturation partial pressure is needed. Table 16 summarizes the vapor pressure for water, DMMP, TBP and MS at room temperature.

Table 16. Saturated Vapor Pressure ($P_{Saturated}$) at Room Temperature

Chemical	$P_{Saturated}$ (mm Hg)
Water	4.54
DMMP	0.34
TBP	0.004
MS	0.0975

6.3.1. Room-temperature Transport of Water Vapor, DMMP, TBP and MS

The results for water, DMMP, TBP and MS transport rate are summarized in Figure 39. The Arkema BCP blend candidates were first screened using water and DMMP and measured TBP and MS permeance for potential candidates. As the results indicate, K1–BCP 88 and K1–BCP 159 blends were identified as our top candidates.

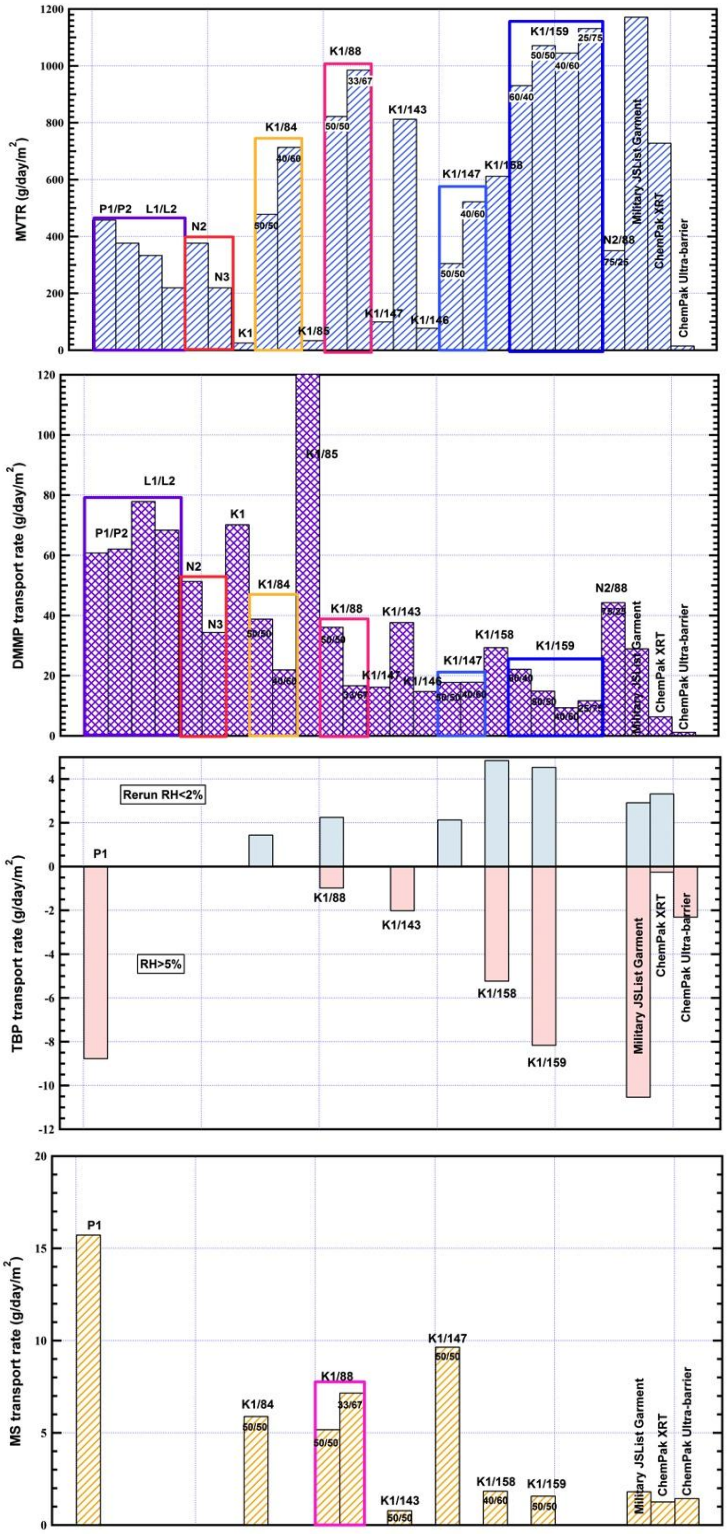

Figure 39. Transport Rate (in g/day/m^2) of Water Vapor, DMMP, TBP and MS through Arkema Membranes in Comparison with JSLIST Material

Note that the transport rates for TBP (RH > 5%) are all negative, suggesting absorption of water moisture from the environment instead of loss of MS through the membranes.

6.3.2. Selectivity of Water Vapor/DMMP, TBP, and MS

The ideal selectivity, which is the ratio of water permeability to that of a chemical simulant, normalized by thickness shows the direct comparison between JSLIST material (benchmark) and Arkema membranes. Due to negative permeability values for TBP, we summarized the selectivity data only for water/DMMP and water/MS (Figure 40).

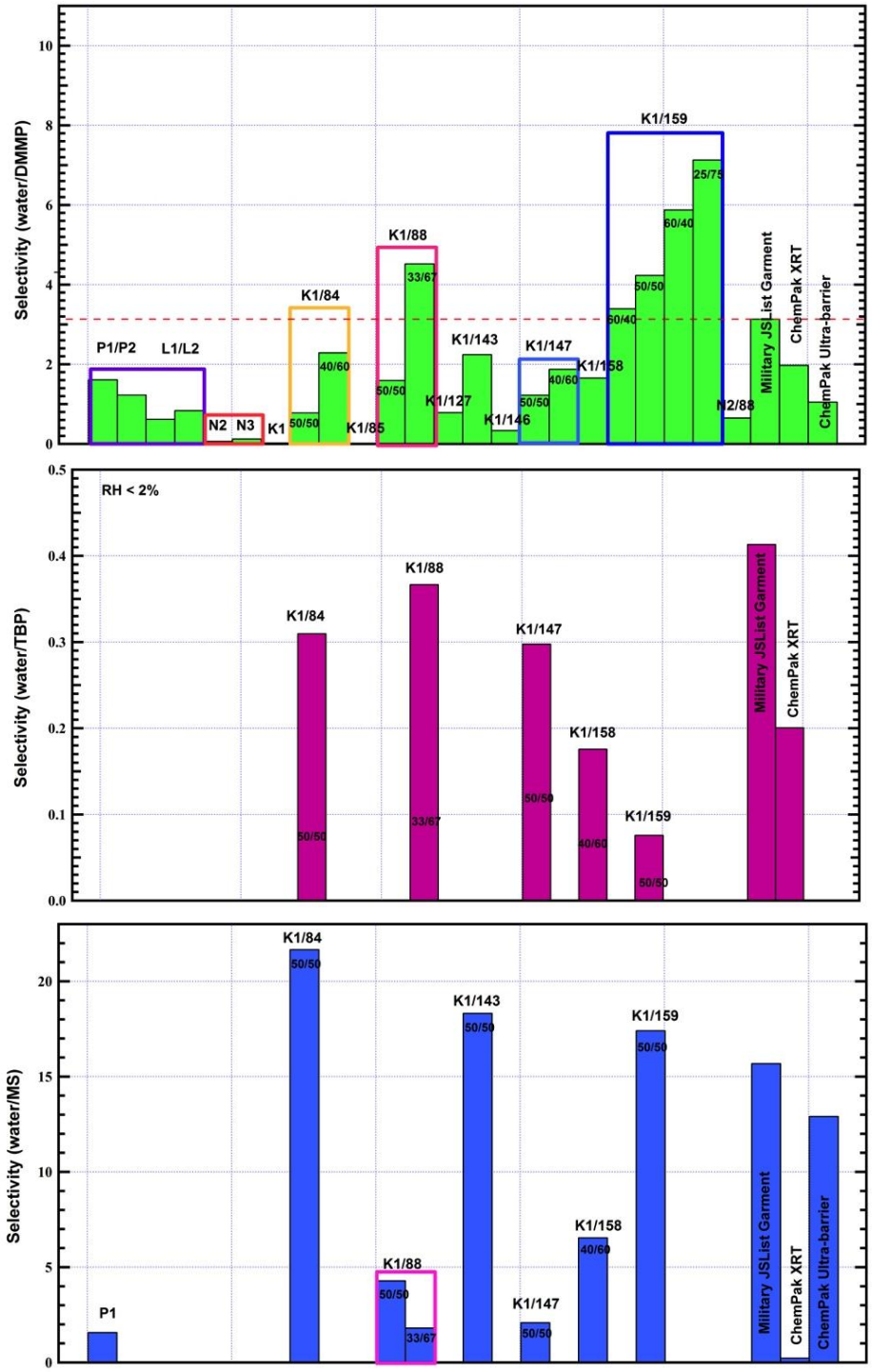

Figure 40. Ideal Selectivity of Water over DMMP, TBP and MS

As shown, the K1–143 and K1–159 blends were top candidates with both higher selectivity of water to DMMP and MS than JSList. K1–88 data were collected only for a 50/50 ratio.

6.3.3. High-temperature Permeability

6.3.3.1. Mocon Temperature Effect Study

The tests run with the Mocon apparatus were usually performed at 37.8 °C (body temperature). A study was done to see if the temperature of the test affected the WVTR values. Table 17 presents values of WVTR obtained for two temperatures (37.8 and 45 °C) on various samples. With an increase of 7 °C in temperature, WVTR values were 1.3 to 2.4 times higher.

Table 17. WVTR Values for Different Temperatures

Block Polymer	wt% BCP	wt% Host	WVTR g.mil/(m^2.day)	TR value g/(m^2.day)	Film thickness mil	Temp. °C
BCP-84	49.8	50.2	**2695**	2406	1.12	37.8
BCP-88	39.9	60.1	**2970**	1880	1.58	
BCP-88	49.9	50.1	**3736**	2442	1.53	
BCP-88	62.5	37.5	**4769**	3117	1.53	
BCP-84	62.5	37.5	**4646**	2640	1.76	
BCP-84	75.0	25.0	**3374**	2359	1.43	
BCP-112	50.0	50.0	**598**	446	1.34	
BCP-115	62.4	37.6	**3196**	2497	1.28	
BCP-84	49.8	50.2	**3681**	3681	1.00	45.0
BCP-88	39.9	60.1	**4050**	2935	1.38	
BCP-88	49.9	50.1	**5660**	3773	1.50	
BCP-88	62.5	37.5	**8713**	5186	1.68	
BCP-84	62.5	37.5	**6779**	4402	1.54	
BCP-84	75.0	25.0	**8220**	5043	1.63	
BCP-112	50.0	50.0	**945**	580	1.63	
BCP-115	62.4	37.6	**7814**	5141	1.52	

6.3.3.2. Permeability Test (cold trap)

The temperature dependence of BCP 88 water flux (Figure 41) was studied by a permeability test using the cold trap method described in 3.3.1.6.

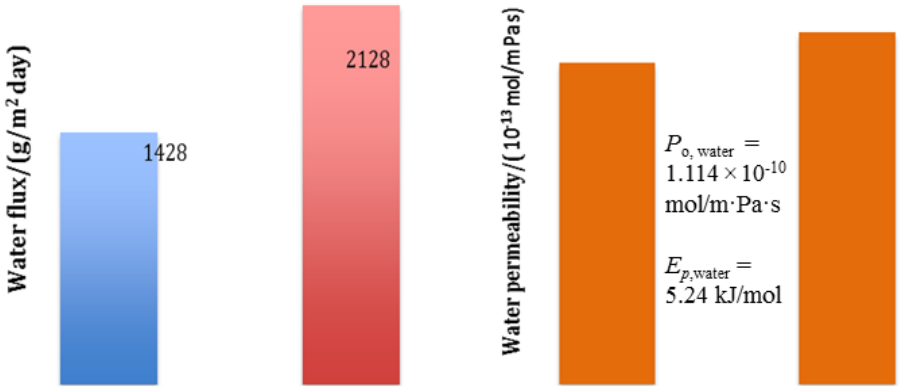

Figure 41. MVTR and Permeability of BCP/K1 (50/50) Membrane at 24 (left) and 37 °C

6.3.4. Permeability and Selectivity Against Water–DMMP Mixture (co-feed)

The K1–88 (33/67) films were examined for permeation of DMMP/water vapor mixtures at 24, 37 and 45 °C, respectively. The films exhibited water vapor fluxes greater than 1,000 g/m^2·day at all three temperatures and water selectivity (over DMMP) of greater than ~4.0 in the first 48 h. The water flux first increased with time (24 ~ 48 h) and then /stabilized; but the water/DMMP selectivity decreased with operation time.

DMMP/water vapor mixture permeation of the K1–88 (33/67) membrane was tested for a total of 130 h of at room temperature. Three permeate samples were collected:

Sample 1: 48 h (0–48 h)
Sample 2: 46 h (48–94 h)
Sample 3: 36 h (94–130 h).

Solutions of DMMP in IPA were prepared with DMMP compositions of 0.0115%, 0.016%, 0.08%, 0.4% and 2%. A 0.5-µL sample of each of these solutions was injected for GC analysis. The GC response spectra were recorded and a calibration curve was determined by correlating the GC peak area with the amount of DMMP injected. To confirm that the zeolite NaA did not adsorb the large molecule DMMP, zeolite NaA was added to the above calibration solutions and the liquid phase was sampled and analyzed by GC again. Results of the GC measurement of the samples before and after addition of the zeolite dehydrating agent were compared in Figure 42. It can be seen that the addition of zeolite particles into the DMMP–IPA solutions did not cause inconsistencies in GC responses to DMMP (i.e. DMMP peak areas) because DMMP is too large to enter the pores of zeolite-A and its adsorption on the zeolite external surface is apparently negligible in the IPA liquid environment. The GC calibration was done by linearly fitting the GC peak area as a function of DMMP injection amount in a range of 0.254 nmol to 63.4 nmol.

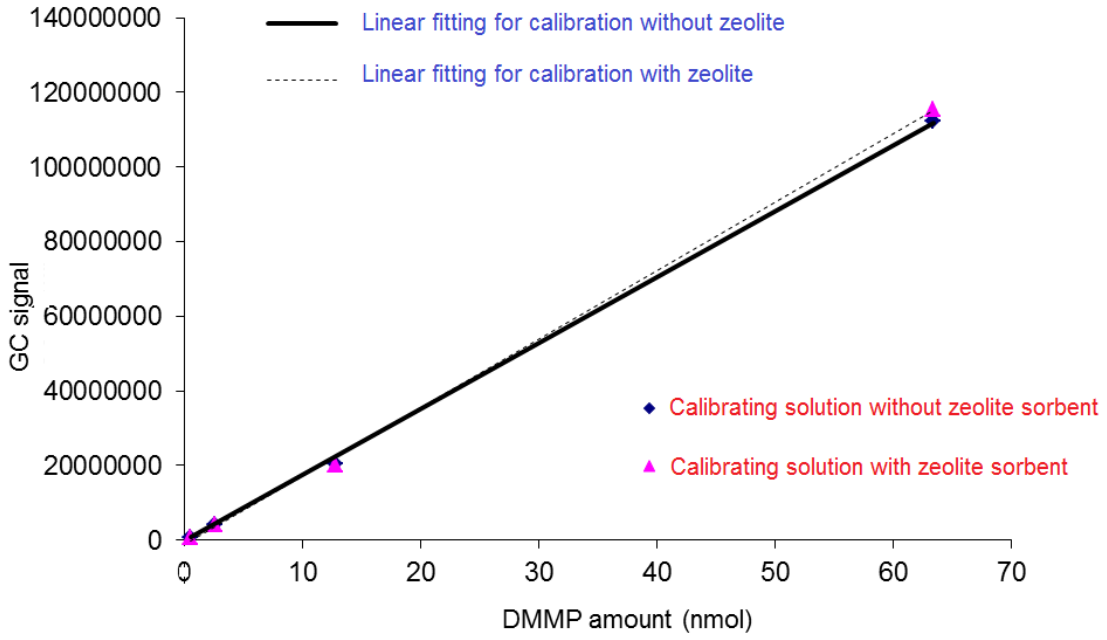

Figure 42. GC Calibrations for DMMP Measurement (Data from Samples with and without the Addition of Particulate Zeolite Sorbents)

The permeation data are represented in Figure 43 for comparison. It should be noted that, because a fresh film was used in permeation test for each temperature, data presented in this figure should not be used to evaluate the temperature-dependence of water flux and selectivity as the three films might have variations in thickness and uniformity. However, it is clear that the films could achieve water vapor fluxes > 1,000 g/m^2·day at all three temperatures with water–DMMP selectivity > 4.0 for the first 48 h.

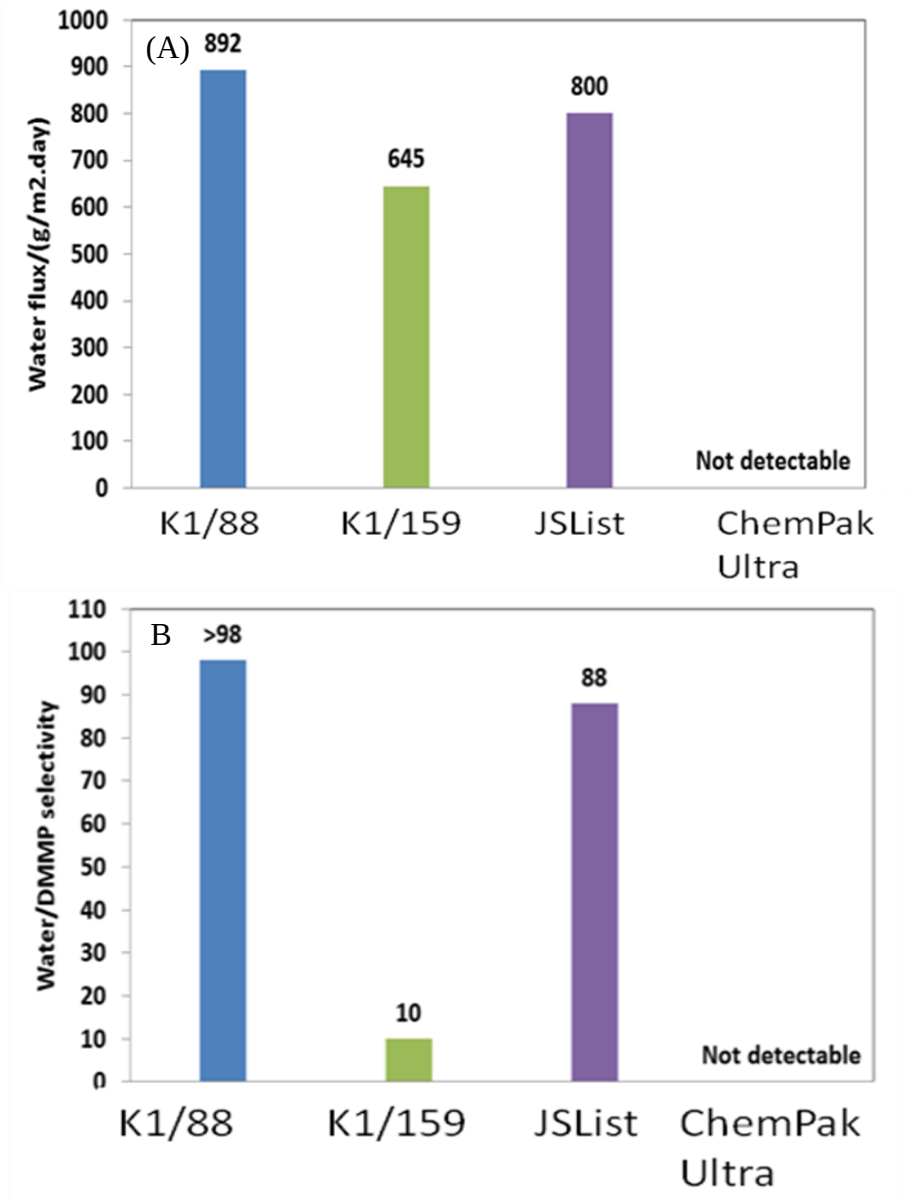

Figure 43. (A) Comparison of Water Flux for Different Membranes and (B) Water/DMMP Selectivity for Different Membranes

Table 18 shows experimental conditions for water/DMMP vapor mixture permeation and the permeation results including water flux, water/DMMP selectivity, and water and DMMP permeance.

Table 18. Permeation of Materials by DMMP (56 Pa)–Water Vapor (1,474 Pa) Mixture after 48 h at 24 °C

Sample name	Sample collected, mg	$a_{H_2O/DMMP}$	J_{H_2O}, g/m^2·day	$P_{m,\ H_2O}$, 10^{-8} mol/s·m^2·Pa	$P_{m,\ DMMP}$, 10^{-8} mol/s·m^2·Pa
K1–88 (33/67)	419.6	>98	892	56.6	<0.1
K1–159 (50/50)	330.6	10.47	645	36.4	2.71
JSLIST	401.0	87.73	800	49.1	0.39
ChemPak Ultra	0	/	0	0	0

6.3.5. Total Heat Loss (THL)

The data shown below are for comparison purposes. The large sweating hot plate test requires a 20 × 20-in material swatch, but our sample testing was performed using 8- × 8-in samples (only 32% of the surface area was covered with test material).

Outside this comparison it is not expected that any extrapolation of values would reliably deliver an accurate comparison to known numbers. Table 19 compiles the THL results.

Table 19. Total Heat Loss by 8 × 8-in Samples of the Most-breathable Films

Sample	wt% BCP	Dry (RCT)	Wet (RET)	Total Heat Loss
Charcoal layer (military pants)	---	0.16	27.0	219.1
BCP 128	50	0.15	36.3	188.5
BCP 112	50	0.13	37.6	196.6
BCP 158	75	0.13	22.5	276.0
BCP 115	62.5	0.14	21.9	269.1
BCP 88	40	0.13	33.0	211.9
BCP 88	50	0.14	22.2	271.3
BCP 88	62	0.14	25.2	247.2
BCP 82	50	0.12	29.1	248.6

The reference chosen, a charcoal layer from a JSLIST BDU, showed a THL of 219 w/m^2. Some of our films out-performed the JSLIST garment with values around 270 (BCP 158, 115 and 88). These results were very encouraging as they indicate better comfort for personnel wearing a garment made from these films. Additional gains could be made during the lamination process. Current testing was performed on prototype layups that left air spaces between layers. These air spaces increased thermal resistance and thereby raised RET values.

6.3.5.1. Small Angle X-ray Scattering (SAXS)

A first series of SAXS analyses showed that:

- crystallinity of K regions was affected by BCP chemistries. For all membranes, crystallinity was seen at 40% and 50% BCP loading, while a few still showed crystallinity at 62.5% loading, illustrating that some BCPs were more compatible than others with K.

- The lowest-*q* scattering peak was likely due to phase separation between K and W1.
- Evidence of BCP structuration was suggested between 0.02 $Å^{-1}$ and 0.06 $Å^{-1}$.
- No obvious correlations were seen between structure and WVTR values. However, one should consider that WVTR values were measured on wet membranes and current studies were based on dry membranes (membranes directly exposed to vacuum conditions).

6.3.5.1.1. Effect of Relative Humidity on K–BCP Structure.

A second series of SAXS experiments were performed using the environmental stage available at the University of Pennsylvania, which allowed for control of humidity up to ~95%. The SAXS peak assignment presented in the first series was confirmed by the environmental measurements. The lowest-*q*-value peak (highest *d*-spacing) was attributed to K–W1 contrast. The lowest-*q*-scattering peak increased for all samples when RH reached 90%. W1 domains were hydrophilic and the presence of water in the W1 domain reduced the electron density of these domains, enhancing contrast with K. Series 88 and 147 showed more change towards lower *q*-values as RH reached 90% (Table 20), indicating an increase in domain size upon water uptake. For the two other series (112 and 128), domain size expansion upon water uptake was subtle to nonexistent.

Table 20. Characteristic Distances in BCP 88 Extracted from $q^2 \times I$ vs. q 1D SAXS Profiles (Series 88)

BCP, %	Env. cond.		q_1 ($Å^{-1}$)	d_1 (nm)	q_2 ($Å^{-1}$)	d_2 (nm)	q_3 ($Å^{-1}$)	d_3 (nm)
	T, (°C)	RH, (%)						
40	24	40	0.010	62.1	0.029	21.5	0.070	9
		90	0.0098	64.4	0.025	25.0	0.070	9
	38	40	0.010	62.1	0.029	21.4	0.070	9
		90	0.0096	65.4	0.027	23.3	0.070	9
50	24	40	0.0097	64.5	0.029	21.4	0.063	10
		90	0.0096	65.3	0.028	22.7	0.063	10
	38	40	0.0097	64.5	0.029	21.4	0.063	10
		90	0.0096	65.3	0.029	22.0	0.063	10
62.5	24	40	0.010	61.4	0.029	22	0.052	12
		90	0.0096	65.3	0.025	25	0.057	11
	38	40	0.010	61.6	0.026	24	0.057	11
		90	0.0098	64.2	0.027	23	0.052	12

NB: In Figs. 56 and 57, membranes with a WVTR value of at least 5,000 g/(m^2.day.mil) are represented with a wider line.

Figures 44 and 45 illustrate the effect of humidity and temperature on peak *d*1 (x-ray scattering contrast between K and W1 block). For almost all samples, humidity had more effect on increasing d1 than temperature (the only exception was for 75% BCP 147).

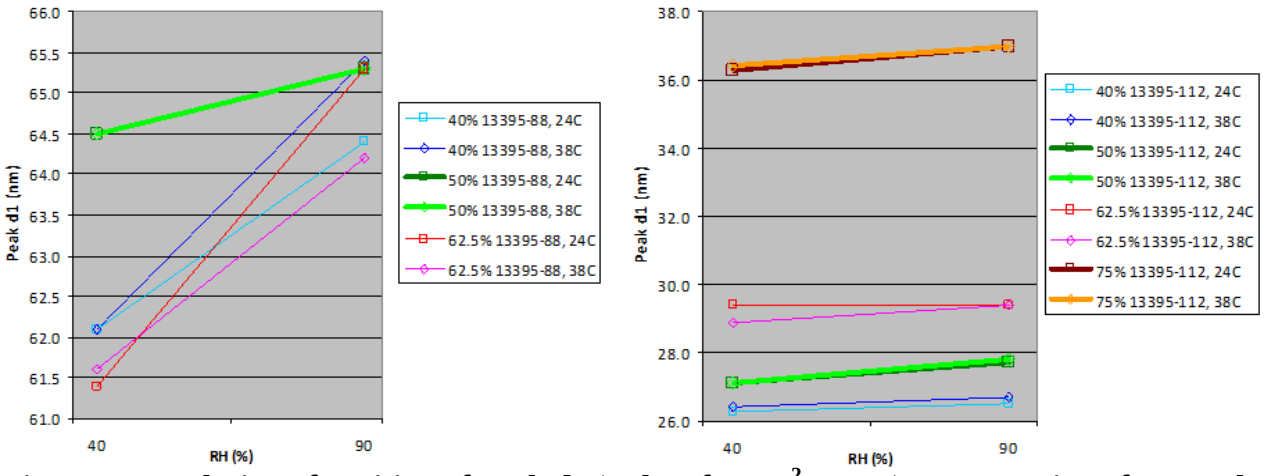

Figure 44. Evolution of Position of Peak *d*1 (Taken from $q^2 \times I$ vs q) as a Function of RH and Temperature for Series 88 (left) and Series 112 (right)

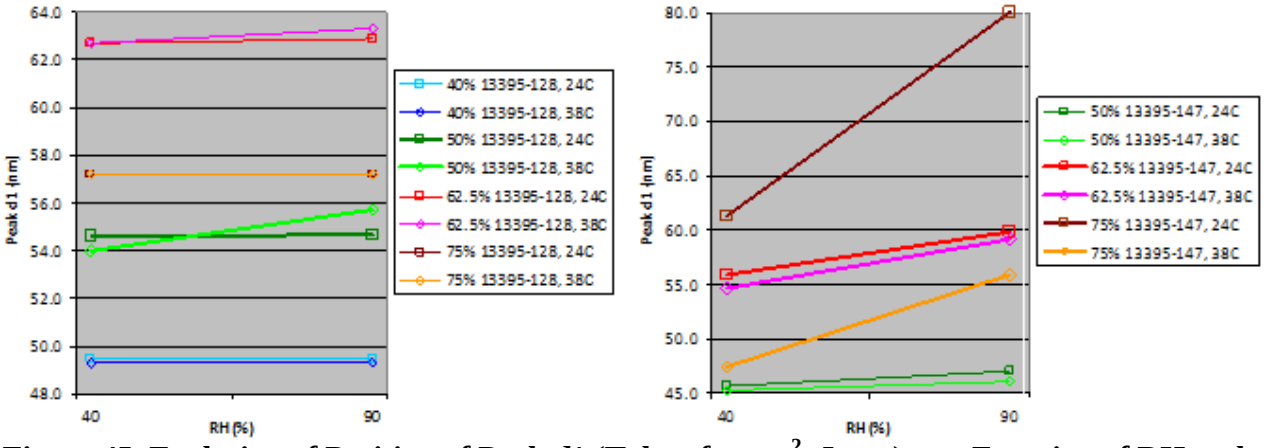

Figure 45. Evolution of Position of Peak *d*1 (Taken from $q^2 \times I$ vs q) as a Function of RH and Temperature for Series 128 (left) and Series 147 (right)

General conclusions could not be drawn across all BCP chemistries. For series 88, the highest WVTR value was obtained for the membrane showing the least *d*1 expansion whereas the opposite was observed for membranes of series 147 (higher WVTR for highest *d*1 expansion). For series 112 and 128 there were no apparent correlations between WVTR and *d*1 change.

6.3.5.1.2. Temperature Effect on K–BCP Structure

For most samples, little effect from temperature value on structure characteristics was observed at 40% RH. Differences were more pronounced when RH was 90%, but the main effect was seen on the intensity of the strongest-scattering peak (lowest *q*-value). The strongest intensity for the lowest-*q*-value peak was seen for the 24 °C experiment (series 88 and 147, both of which had similarities in their block copolymer relative ratio) or for the 38 °C experiment (series 112 and 128). Notice, however, intensity variations as a function of temperature for series 112 and 128 were much less pronounced than were seen for series 88 and 147.

7. MODELING

7.1. Water and DMMP Permeability Mechanism by Single-gas Permeability Test

The perm-selectivity (also called *ideal selectivity*, $\alpha^0_{H_2O/i}$) is defined as the permeance ratio of water vapor over other gases (was calculated based on the water vapor and single-gas permeability results (Table 21)). The results for a BCP N2 membrane are summarized in Table 22. The results show that BCP N2 is very selective of water over other gases. However, it should be pointed out that the ideal selectivity was often unable to predict the selectivity for gas mixture permeation. For example, if the polymer is oleophilic, the preferential adsorption of organics could block or hinder water molecule transport and reverse the membrane to organic selective. This possibility will be tested and discussed in the future. The effect of preparation conditions on the membrane permeation properties was inconclusive due to the limited experimental data.

Table 21. Gas Permeance and Permeability Results for BCP N2 Membrane

Membrane (Thickness, μm)	Permeance ($\times 10^{-10}$ mol/m^2·Pa·s)			Permeability ($\times 10^{-13}$ mol/m·Pa·s)		
	N_2	CH_4	*i*-C_4H_{10} (Isobutane)	N_2	CH_4	*i*-C_4H_{10} (Isobutane)
BCP N2 dried at 90 °C under vacuum (38)	3.27	0.723	3.05	0.12	0.28	0.12
BCP N2 annealed at 120 °C (77)	0.114	0.956	3.24	0.088	0.07	0.25
BCP N2 dried at room temperature under vacuum (47)	1.36	0.476	2.56	0.064	0.02	0.12
BCP N2 dried at 80 °C under vacuum (51)	0.134	1.07		0.007	0.06	
PMMA membrane from literature				0.039 Ba* [1] 0.2 Ba* [2]	0.009 Ba *[2]	

[1] Y. Nakai, H. Yoshimizu, Y. Tsujita, Enhancement of Gas Permeability in HPC, CTA and PMMA under Microwave Irradiation, *Polymer Journal* 38 (2006) 376.
[2] W.J. Koros, G.K. Fleming, S.M. Jordan, T.H. Kim, H.H. Hoehn, Polymeric membrane materials for solution-diffusion based permeation separations, *Prog. Polym. Sci.* 13 (1988) 339.
*: Ba = Barrer (1 Barrer = 3.348 x 10^{-16} mol m / (m^2 s Pa))

Table 22. Perm-Selectivity* of Water Vapor over Another Gas *i* ($\alpha^0_{H_2O/i}$) through 38-μm BCP N2 Membrane Dried at 90 °C under Vacuum

Selectivity ($\alpha^0_{H_2O/i}$), dimensionless		
N_2	CH_4	Isobutane
296	134	318

*Selectivity is defined as the ratio of pure-gas permeances (data from Table 21)

The results from single-gas tests (Table 21) show that permeability decreased with kinetic diameter of the small gas molecules (H_2O, N_2, CH_4), but increased for isobutane, suggesting a

sorption-dominated permeation mechanism for isobutane (i.e., large solubility *S* but small diffusivity *D*) but diffusion-dominated for small and weakly adsorbing gases (i.e., small *S* and large *D*). More tests are necessary to determine the permeation mechanisms for all gases.

Permeability data for single gases (He, H_2O, CO_2, N_2, CH_4, isobutene), DMMP and water were collected for BCP N2 membranes of varied thickness (Figure 46). As seen for water and DMMP, permeability deviated upwards from the kinetic diameter linear relationship suggesting a permeation mechanism dominated by sorption. Molecular simulation on a BCP N2 system (Figure 47) also indicated that DMMP and water are much more soluble than single gases, deviating from the

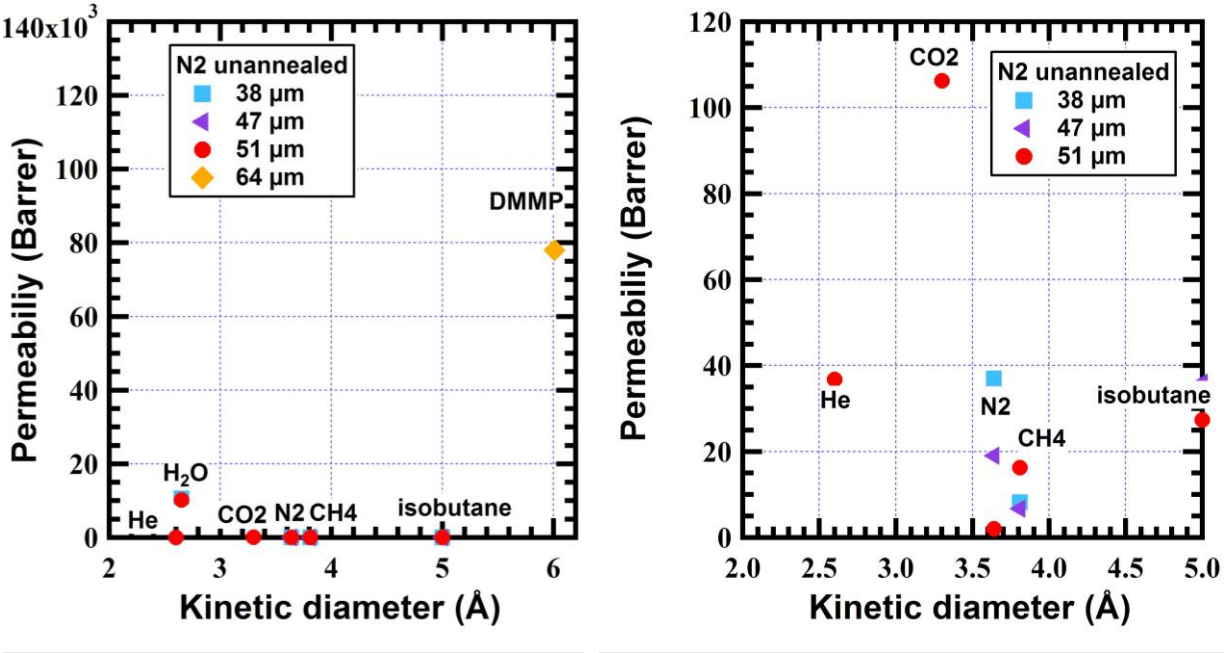

Figure 46. Single-gas Permeability as a Function of Kinetic Diameter of Permeates Including (left) and Excluding (right) DMMP and Water

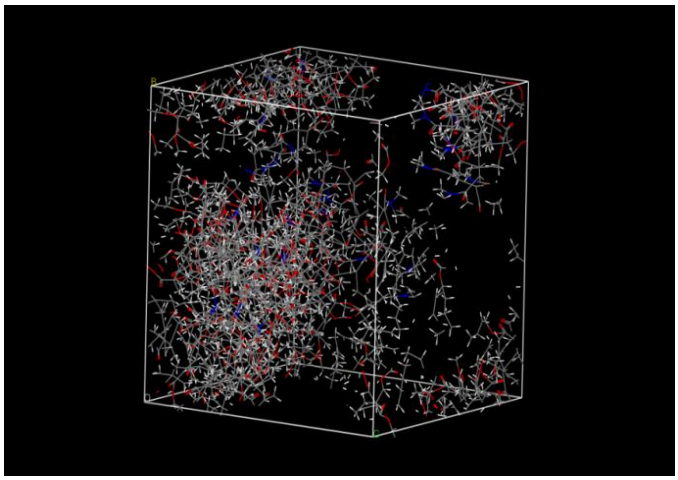

Figure 47. A Representative Simulation System with 200 Repeat Units of BCP N2 in a Periodic Cube

trend with kinetic diameter (e.g., the diameter of water is smaller than of CO_2 and CH_4, but solubility is much higher) as shown in Figure 48. Therefore, the dominant permeability mechanism was sorption. More focus on modeling of sorption will be described in the following sections.

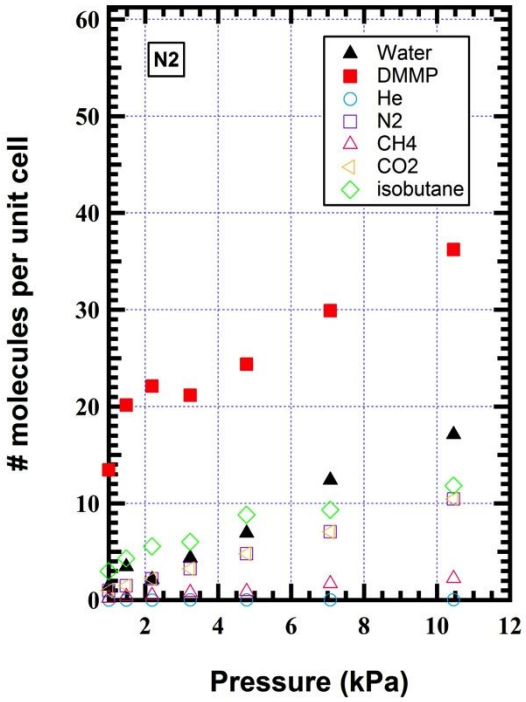

Figure 48. Sorption Results from GCMC Calculation for Single Gases by BCP N2

7.2. HSP Calculation Based on Group Contribution

Tests were conducted to model two commercial BCPs. The HSP (Table 23**)** was calculated based on the number of functional groups in the BCPs (Table 24).

Table 23. Calculated HSP Values

BCP	δ_d (MPa)	δ_p (MPa)	δH (MPa)
N2	14.94	6.94	8.99
N3	14.51	6.22	9.03

Table 24. Number of Group Contributions in Two BCPs

groups	MMA	BA	DMA	N2	N3
CH3	2	1	2	750	1214
- CH2 -	1	4	1	1110	1482
> CH -	0	1	1	292	396
>C<	1	0	0	188	336
> C=O	1	1	1	480	732
- O -	1	1	0	398	586
-N<	0	0	1	82	146

Water and DMMP selectivity was predicted from the model as shown in Table 25. The simulation results on selectivity of BCPs N2 and N3 are compared with experimental data in Figure 49.

Table 25. Selectivity of Two BCPs

	$\Delta\delta$(BCP, H_2O)*	$\Delta\delta$(BCP, DMMP)	Selectivity
N2	34.54	7.25	0.21
N3	34.74	8.30	0.24

*** $\Delta\delta$ is the difference in solubility parameter between solvent and host (Eqs. (15) and (16)).**

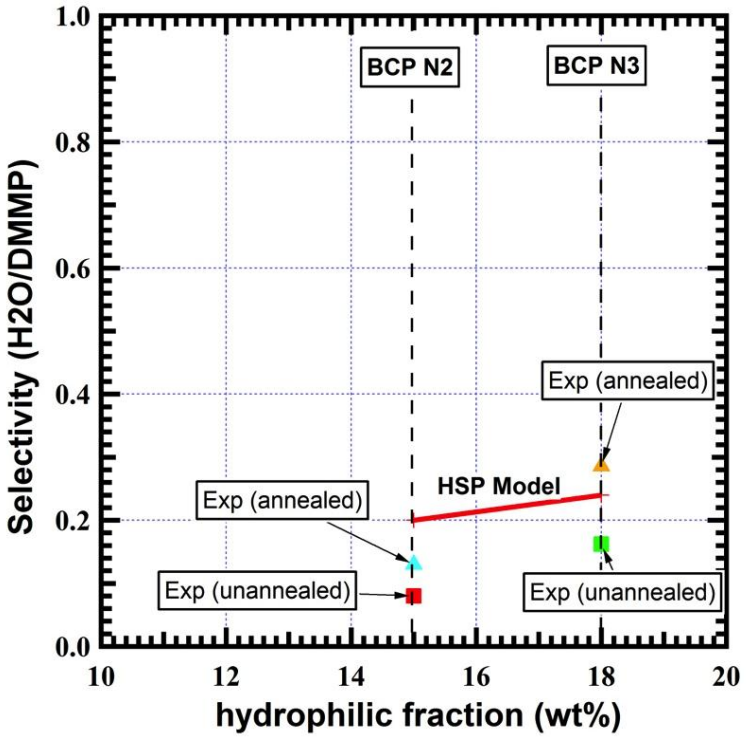

Figure 49. HSP Model Prediction of Water/DMMP Selectivity on BCPs N2 and N3 Compared with Experimental Data

For both N2 and N3, annealed samples showed higher selectivity than unannealed samples, suggesting fewer defects after annealing. HSP model prediction on selectivity followed the experimental results of dependence on hydrophilic fraction in the BCPs.

After validation on BCPs N2 and N3, the HSP model was used to predict the membrane blends studied by the permeability tests. The results on a representative blend K1–159 as a function of K1 and BCP 159 ratio are shown in Figure 50. The HSP model under-predicted the selectivity.

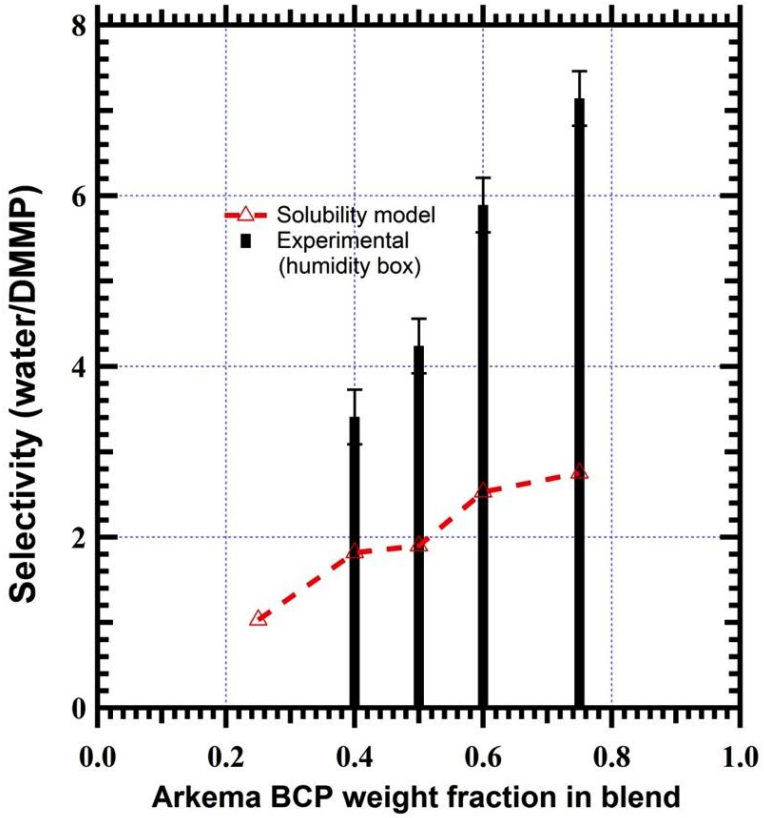

Figure 50. HSP Model Prediction (Red Dashed Line) Compared with Experimental Measurement (at RT) on K1–159 as a Function of BCP Weight Fraction in the Blend.

7.3. Diffusion Correction

A diffusion correction based on domain size was used to modify the permeability calculation in our model. The sizes for hydrophilic and hydrophobic domains were determined using the following two methods.

7.3.1. Domain Size Calculated by Chain Length (Corrected Random Walk)

A parameter *k* was used to correct the domain size prediction based on the random walk assumption.

$$R = n^k \times b,\ 0.5 \leq k \leq 1.0 \qquad (18)$$

Assuming a *k* value, the domain size was then computed and plugged into Eq (18) to correct the diffusion coefficient. The selectivity then can be calculated for K1–159 as a function of BCP 159 weight faction (Figure 51).

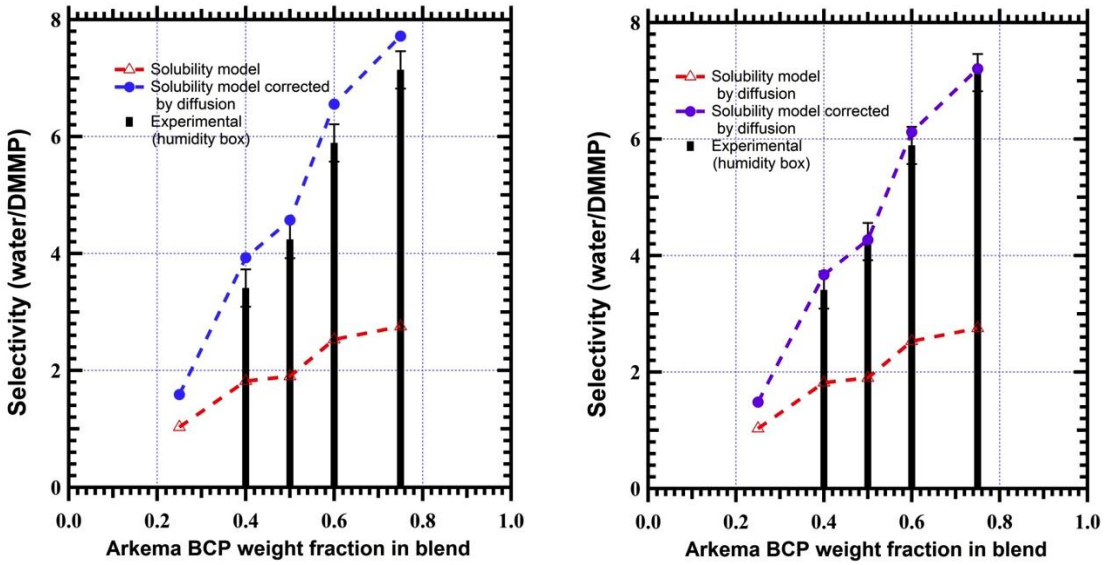

Figure 51. Diffusion-Corrected HSP Model Prediction after Diffusion Correction by Chain Length Calculation

(k = 1.0 left, and k = 0.7 right) compared to experimental results as well as HSP model before diffusion correction. k = 0.7 (right) is the optimal parameter for diffusion correction

7.3.2. Domain Size Calculated from SANS Data

Analysis of the SANS data revealed morphological information including the domain size for both hydrophilic and hydrophobic domains. The SANS results (Figure 52) on domain sizes of K1–159 generated by characterization described in 6.2.3. were used to correct the effect of domain size on diffusivity and therefore selectivity. The results as a function of BCP weight fraction are shown in Figure 53. Domain size increased with BCP weight fraction, following the trend of selectivity.

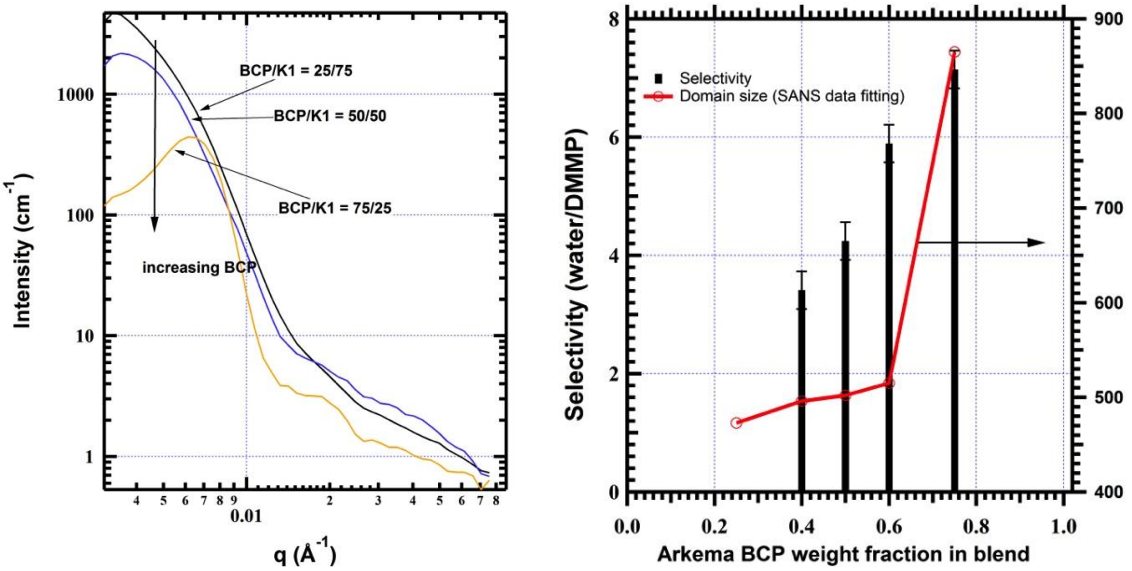

Figure 52. SANS Data (left) and Correction between Selectivity and Domain Size from Fitting of SANS Data (right)

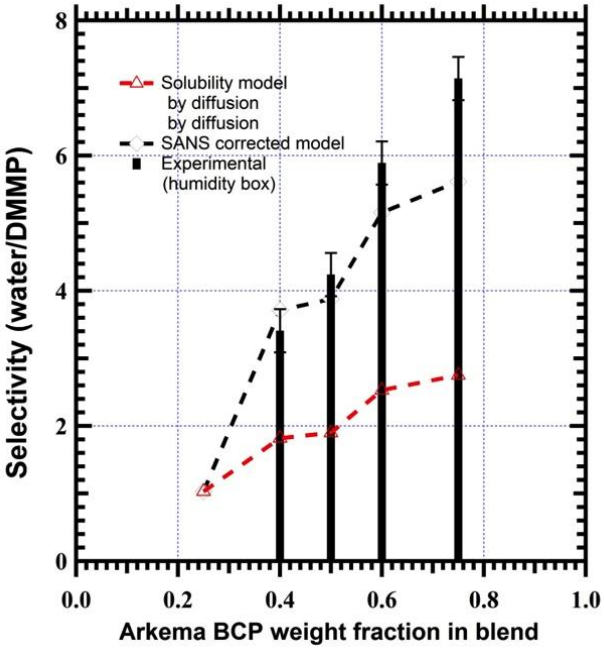

Figure 53. Water/DMMP Selectivity as a Function of Weight Fraction of BCP 159 in Blend with K1

7.4. HSP Model Combined with Diffusion Correction

The final UC model (model developed at University of Cincinnati) was used to predict the water/DMMP selectivity of most BCP–K1 blends in this study. The model predictions are compared with experimental measurements at RT as shown below.

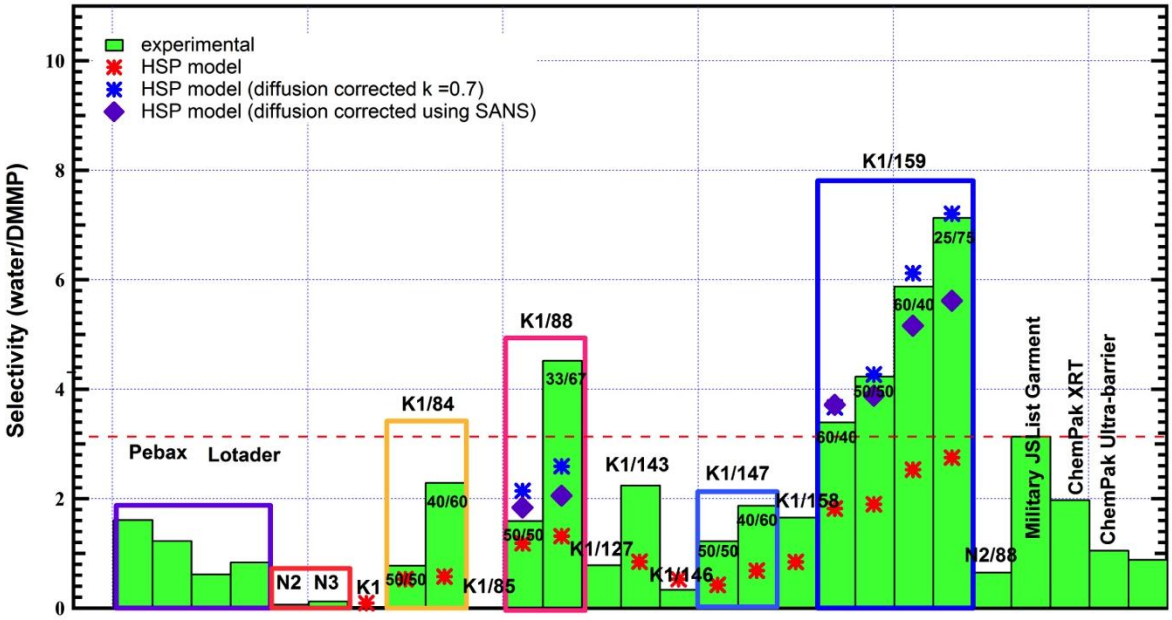

Figure 54. UC Model Predictions Compared with Experimental Data. The Final UC Model (HSP Combined with Diffusion Correction (k = 0.7)) is the Optimal Model

8. OPTIMIZATION

We established a reliable computational model at UC (based on Hansen solubility parameter and group contribution calculation in combination with diffusion correction) to optimize the chemical composition of the BCPs. This model has been validated by experimental results on permeability and selectivity measurement of a series of Arkema BCPs. We focused on two groups of Arkema PMMA-based BCPs as the targets for optimization.

8.1. Optimization on BCP Group 1

The Group 1 polymers are the Arkema BCPs synthesized by Route 1. The structure–property relationship (relationship between BCP chemical compositions and selectivity) for the first group of Arkema BCPs is demonstrated in Figure 55. As shown, for Arkema BCPs to outperform JSLIST, the hydrophilic (W1) mol% must be higher than 35% for a total BCP molecular weight of 75,000 kDa. However, increasing the W1 ratio decreased the solubility of BCP in the casting solvent (DMSO) (see Figure 56).

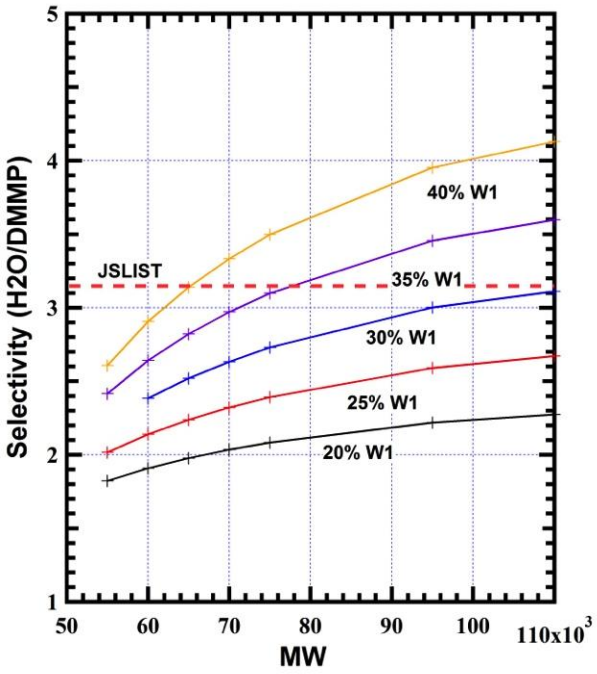

Figure 55. Structure–Property Relationship (from the UC Model) Correlating Selectivity to Total Molecular Weight and the W1 Mol Ratio (in Final BCP Structure)

The higher the HSP, the more difficult will be free-solvent casting the BCP into standalone membranes. Based on our experimental experience, the HSP for Arkema BCPs should be lower than 28.0 to achieve good film quality (dotted line).

Based on the UC model, decreasing B1/B2 ratio and molecular weight of the first block can also slightly increase the H_2O/DMMP selectivity. Combining correlation shown in Figures 55 and 56, UC model predicts an optimized structure for BCP 6.

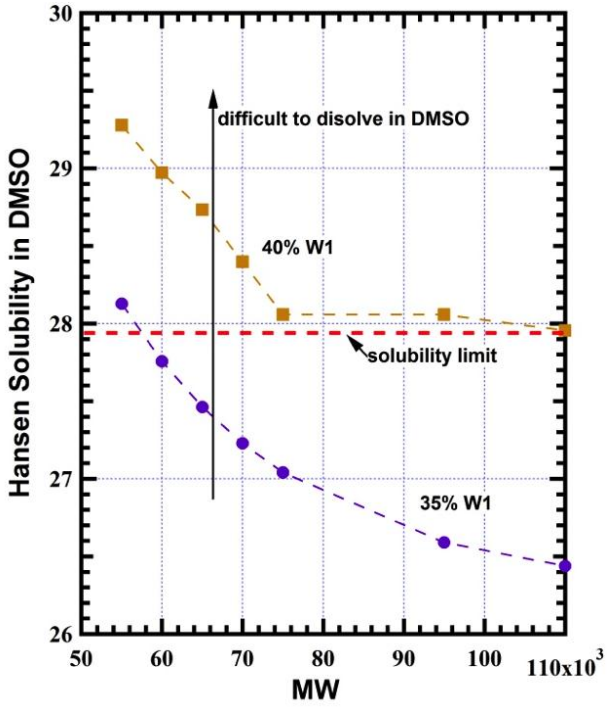

Figure 56. Hansen Solubility Parameter Correlated to the Total Molecular Weight and the W1 Mol Ratio (in Final BCP)

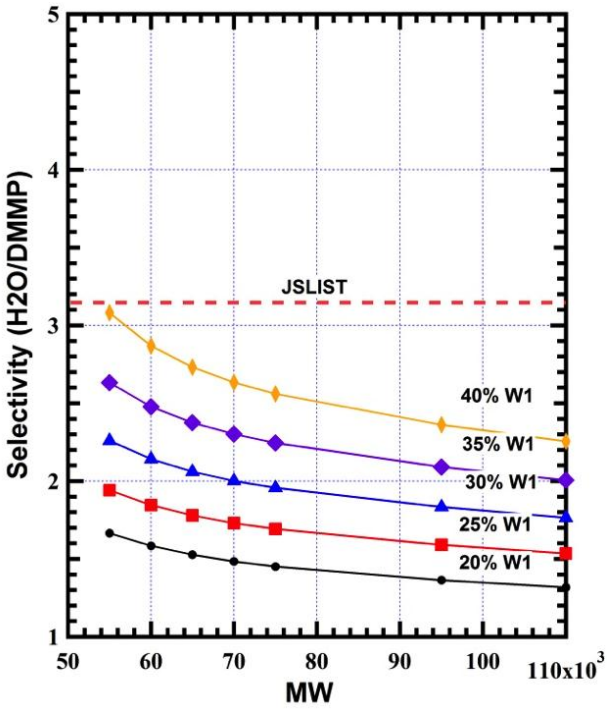

Figure 57. Structure–Property Relationship Correlating Selectivity to Total Molecular Weight and W1 Mol Ratio (in Final BCP) in Arkema BCPs (by Second Synthetic Route)

8.2. Optimization on BCP group 2

The second group of Arkema BCPs showed a different structure–property trend (Figure 57) from the first group. As shown, the selectivity decreased as total molecular weight increased. In addition, compared to the first group, these BCPs showed lower selectivity at the same W1 mol fraction in the final BCPs.

As the second group of BCPs generally showed better solubility in DMSO (HSP parameters lower than 27), we thought it worth trying to optimize this group of BCPs. Therefore, we propose a theoretically optimized structure named as BCP 5 (40% W1, MW 45kDa).

8.3. Performance of Optimized BCPs

The MVTR of the two new BCP blends (at 50/50 weight ratio to K1) are compared with the previous measured membranes in Figure 58. As shown, K1–6 showed a high potential with a MVTR of 800 g/day/m^2 at room temperature and film mechanical strength was not compromised.

K1–6 showed a higher MVTR than both GoreTex products (ChemPak XRT and ChemPak Ultra) at similar film thickness. BCP 159–88 showed the highest MVTR; however, its mechanical properties were not as good.

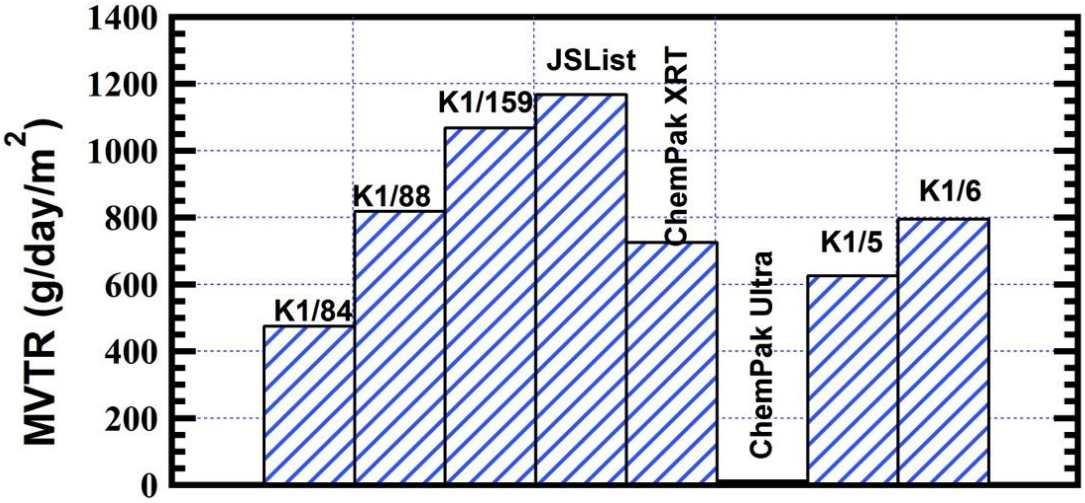

Figure 58. MVTR of K1–5 and K1–6 Compared with Previously Studied Arkema BCPs at Same Weight Ratio

The selectivity of BCP blends is compared in Figure 59, which normalized the difference in film thickness, isolating the properties of the materials.

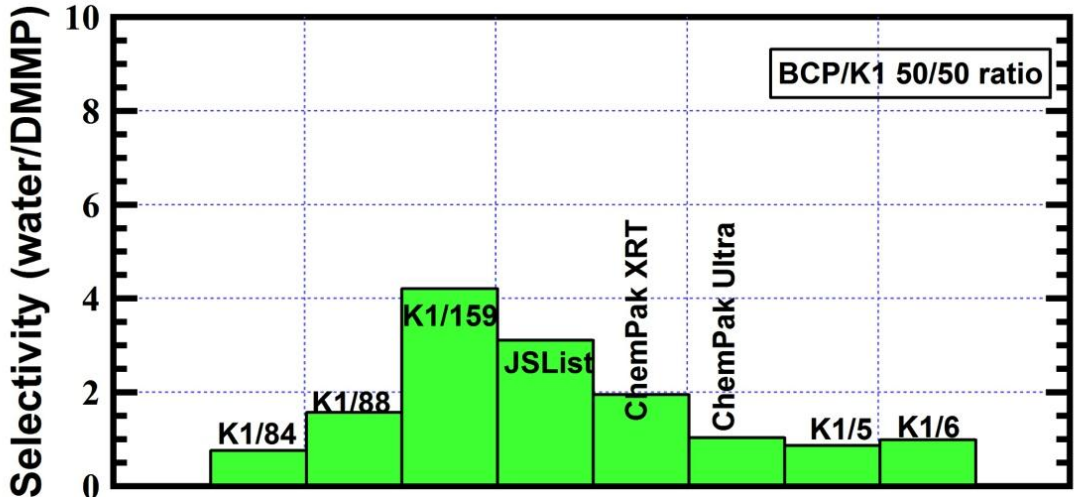

Figure 59. Water/DMMP Selectivity of BCP 5 and BCP 6 Compared to Previously Studied BCPs. K1–6 Shows Selectivity Comparable to That of ChemPak XRT

9. CONCLUSIONS AND RECOMMENDATIONS

9.1. Conclusions

Successfully synthesized potential barrier materials based on Arkema BCPs exceeded current technology for protective garments. The new SPMs (BCP 88–K1) showed a combination of high THL, high WVTR (same level as JSLIST) and comparable water selectivity. A model that implemented group contribution calculation of the Hansen solubility parameter was established, and included a morphology correction. This model was also validated by experimental permeability measurements on a series of Arkema BCP blend membranes, and has been used to predict optimal structures.

The approach integrating of synthesis at Arkema, modeling at UC and performance evaluation at Arkema, UC and Lion has proven to be a successful and efficient strategy to screen and develop a new material for the goals of this project.

9.2. Recommendations

The final deliverables of this project (BCP 88–K1 blend membranes) are believed to perform better in combination with non-woven fabric materials as substrate in terms of water resistance, liquid chemical simulant repulsion, and mechanical strength. We recommend continuing this project, following optional years 2 and 3, as described in this first-year contract.

10. REFERENCES

1. Lu, X. Y.; Nguyen, V.; Zhou, M. J.; Zeng, X. H.; Jin, J. Z.; Elliott, B. J.; Gin, D. L., Crosslinked bicontinuous cubic lyotropic liquid-crystal/butyl-rubber composites: Highly selective, breathable barrier materials for chemical agent protection. *Adv Mater* 2006, *18* (24), 3294-+.

2. (a) Kroschwitz, J. I., *Kirk-Othmer encyclopedia of chemical technology*. 5th ed.; J. Wiley: Hoboken, N.J., 2004; p v; (b) Satas, D., *Coatings technology handbook*. M. Dekker: New York, 1991; p xvi, 784 p.

3. Wartell, M. A., *Strategies to protect the health of deployed U.S. forces : force protection and decontamination*. National Academy Press: Washington, D.C., 1999; p xxii, 238 p.

4. Alexandroff, E. E., *"Saratoga carbon pellet technology in chemical warfare protective clothing" in the Proceedings of the Second International Symposium on Protection Against Chemical Warfare Agents*. Swedish Defence Research Institute, Department of NBC Defence: Umeå,Sweden, 1986; Vol. 15-19.

5. (a) Alexandroff, E. E., *"PBI Saratoga new and improved CWU/66p chemical protective clothing system for aircrew application" in Proceedings of the Third International Symposium on Protection Against Chemical Warfare Agents*. Swedish Defence Research Institute, Department of NBC Defence: Umeå,Sweden, 1989; Vol. 11-16; (b) Helper, E., *"The new personal chemical protective suit of the U.S military services" in Proceedings of the Sixth International Symposium on Protection Against Chemical Warfare Agents*. Swedish Defence Research Institute, Department of NBC Defence: Umeå,Sweden, 1998; Vol. 10-15.

6. Maroldo, S. G., *"Carbonaceous resins-sorbents for chemical protection" in Proceedings of the Third International Symposium on Protection Against Chemical Warfare Agents*. Swedish Defence Research Institute, Department of NBC Defence: Umeå,Sweden, 1989; Vol. 11-16.

7. Shishoo, R., Recent developments in materials for use in protective clothing. *International Journal of Clothing Science and Technology* 2002, *14* (3), 201-215.

8. ASTM Standard E96E, Standard Test Methods for Water Vapor Transmission of Materials In *Annual Book of ASTM Standards*, The American Society for Testing and Materials: West Conshohocken, PA, 2003; Vol. 04.06.

9. ASTM Standard D1434, Standard Test Method for Determining Gas Permeability Characteristics of Plastic Film and Sheeting. In *Annual Book of ASTM Standards*, The American Society for Testing and Materials: West Conshohocken, PA, ; Vol. 15.09.

10. Ilavsky, J.; Jemian, P. R., Irena: tool suite for modeling and analysis of small-angle scattering. *J Appl Crystallogr* 2009, *42*, 347-353.

11. Hansen, C. M., *Hansen solubility parameters : a user's handbook*. CRC Press: Boca Raton, Fla., 2000; p 208 p.

12. Sun, H., COMPASS: An *ab initio* force-field optimized for condensed-phase applications - Overview with details on alkane and benzene compounds. *J Phys Chem B* 1998, *102* (38), 7338-7364.

LIST OF SYMBOLS, ABBREVIATIONS, AND ACRONYMS

ASTM 96E	American Standard Test Methods for Water Vapor Transmission of Materials
ASTM D1474	American Standard Test Methods for Determining Gas Permeability Characteristics of Plastic Films and Sheeting.
Barrer	permeability unit: 3.348×10^{-19} kmol m / (m^2 s Pa)
BCP	block copolymer
COMPASS	Condensed-phase Optimized Molecular Potentials for Atomistic Simulation Studies
CWA	chemical warfare agent
DMMP	dimethyl methylphosphonate
DMSO	dimethyl sulfoxide
GCMC	grand canonical Monte Carlo
GC	gas chromatography
HPLC	high-performance liquid chromatography
HSP	Hansen solubility parameter
IPA	isopropyl alcohol
ISO	International Organization for Standardization
MS	methyl salicylate
MVTR	moisture vapor transport rate
NFPA	National Fire Protection Association
NR	neutron reflectivity
NPT	ensemble using fixed values of number of atoms, pressure and temperature
RH	relative humidity
SANS	small-angle neutron scattering
SAXS	small-angle X-ray scattering
SPM	semipermeable membrane
TBP	tributyl phosphate
THL	total heat loss
WVTR	water vapor transport rate (same as MVTR)

INDEX